Journal of Orthopaedic Translation 50 (2025) 274–294

Contents lists available at ScienceDirect

Journal of Orthopaedic Translation

journal homepage: www.journals.elsevier.com/journal-of-orthopaedic-translation

Humanin reduces nucleus pulposus cells ferroptosis to alleviate intervertebral disc degeneration: An in vitro and in vivo study

Daxue Zhu [a,b,1], Zhaoheng Wang [a,b,1], Yanhu Li [a,b,1], Shijie Chen [a,b], Xuewen Kang [a,b,*]

[a] Lanzhou University Second Hospital, 82 Cuiyingmen, Lanzhou, 730030, PR China
[b] Key Laboratory of Orthopedics Disease of Gansu Province, Lanzhou University Second Hospital, 730030, PR China

ARTICLE INFO

Keywords:
Ferroptosis
HSP27
Humanin
Intervertebral disc degeneration
Necleus pulposus

ABSTRACT

Background: Intervertebral disc degeneration (IDD) is a prevalent etiology of low back pain in the global adult population, leading to considerable morbidity and healthcare costs. Existing therapeutic modalities for IDD remain constrained. Ferroptosis in the nucleus pulposus (NP) cells emerges as a pivotal contributor to IDD. Humanin (HN), a mitochondrial-secreted peptide, is intricately linked to age-related maladies and showcases antioxidant, anti-inflammatory, and anti-apoptotic properties. Nonetheless, its precise involvement in IDD remains enigmatic.

Methods: The expression profile of HN in IDD was scrutinized utilizing human NP cell cultures and an IDD rat model (n = 5). The therapeutic efficacy of HN in rats was assessed via MRI and histological evaluation, alongside an exploration of the molecular underpinnings of HN's therapeutic actions in IDD management.

Results: This pioneering study unveiled a downregulation of HN expression in IDD patients, a finding corroborated through cell and rat IDD models. Furthermore, it was ascertained that exogenous HN could trigger endogenous HN expression, impede the JAK2/STAT3 and NF-κB pathways, thereby mitigating erastin-induced ferroptosis in NP cells, contingent upon the upregulation of HSP27 expression. Moreover, the study validated the role of HN in preserving mitochondrial homeostasis, curbing mitochondrial reactive oxygen species (mtROS) generation and mtDNA leakage, consequently hindering mtDNA binding to TLR9 and subsequent activation of the NF-κB pathway. Notably, in vivo rat experiments underscored the efficacy of HN treatment in ameliorating IDD progression induced by annulus fibrosus puncture.

Conclusion: By assuaging ferroptosis in NP cells, HN exhibits promise as a viable candidate for IDD treatment, capable of impeding disease advancement. **The translational potential of this article**: This study highlights the importance and effectiveness of HN in alleviating IDD by inhibiting ferroptosis in NP cells. The addition of exogenous HN may represent a potential therapeutic strategy for treating IDD.

Abbreviations:

AF	Annulus fibrosus
CEP	Cartilage endplate
DEGs	Differentially expressed genes
ECM	Extracellular matrix
GSH	Glutathione
KEGG	Kyoto Encyclopedia of Genes and Genomes
Humanin	HN
IHC	Immunohistochemistry
IDD	Intervertebral disc degeneration
IVD	Intervertebral disc
MMP	Mitochondrial membrane potential
mtDNA	Mitochondrial DNA
mtROS	Mitochondrial reactive oxygen species
mPTP	Mitochondrial permeability transition pore
NP	Nucleus pulposus
NS	Normal saline
ROS	Reactive oxygen species
MDA	Malondialdehyde
MMP	Mitochondrial membrane potential

* Corresponding author. Lanzhou University Second Hospital, 82 Cuiyingmen, Lanzhou, 730030, PR China.
E-mail address: ery_kangxw@lzu.edu.cn (X. Kang).
[1] These authors contributed equally.

https://doi.org/10.1016/j.jot.2024.12.002
Received 5 July 2024; Received in revised form 30 September 2024; Accepted 9 December 2024

1. Introduction

Low back pain is a common musculoskeletal disorder, with an intervertebral disc (IVD) degeneration (IDD) being a major contributor to its development, imposing significant economic burdens on patients and society [1,2]. Due to the worsening trend of aging population, the prevalence of this condition is rapidly increasing, estimated to affect around 37 % of adults worldwide, which poses a significant challenge to public health programs and is an urgent global public health concern [3]. Furthermore, IVD plays a crucial role in connecting the soft tissues of the spinal vertebrae, consisting of the nucleus pulposus (NP), annulus fibrosus (AF), and cartilage endplate (CEP) [4]. Various factors, such as age, injury, and immune responses, lead to various structural changes within the IVD, including reduced disc height, NP cells apoptosis, AF ruptures, CEP calcification, and imbalances in extracellular matrix (ECM) metabolism, particularly focusing on impaired NP cells function and decreased cell numbers within the IVD [5,6]. On the contrary, ferroptosis, characterized by cell death due to cellular iron overload, has emerged as a significant contributor to the progression of IDD [7]. Notably, recent studies have emphasized the role of ferroptosis in mediating IDD, where iron-mediated lipid peroxidation induces mitochondrial abnormalities in NP cells, significantly affecting cell damage or death within the IVD, suggesting ferroptosis to be a potential novel therapeutic target for IDD [8,9].

Humanin (HN), a 24-amino acid peptide encoded by the 16S ribosomal RNA gene MTRNR2 within the mitochondrial genome, has attracted attention for its cellular protective properties [10]. Several studies have clarified that HN and its derivative can alleviate oxidative stress, counteract mitochondrial dysfunction, reduce ROS levels, and exhibit anti-inflammatory, anti-oxidant, and anti-apoptotic effects in various organs [11,12]. An analog of HN identified in rats, called Rattin, shows similar protective effects to human HN [13]. Moreover, studies have shown age-related declines in HN levels across rodents, primates, and humans, suggesting a plausible connection between insufficient HN levels and age-associated diseases [14,15]. Further investigations and researches have confirmed that administering exogenous HN or its derivative helps alleviate symptoms of oxidative stress-related degenerative aging, including neurodegenerative diseases, type 2 diabetes, cardiovascular diseases, memory impairment, stroke, inflammation, and amyotrophic lateral sclerosis [16,17]. In addition, HN has been implicated in protecting growth plate chondrocytes from apoptosis induced by glucocorticoids [18]. Recent studies have shed light on additional biological effects of HN, as it significantly inhibited decreased cell viability and ROS generation, while also leading to a marked increase in the protein levels of GPX4, a key regulator in ferroptosis [19]. Therefore, we hypothesize that exogenous supplementation of HN may delay IDD by reducing ferroptosis in NP cells. However, the expression of HN in IDD and its potential protective effects on NP cells remains unclear and warrant further investigation.

HSP27, also known as HSPB1, is a small heat shock protein that belongs to the small heat shock protein family and is widely expressed in mammalian cells, especially in tissues such as muscles, nerves, and lenses [20,21]. Takao et al. [22] demonstrated that HSP27 is localized to the nuclei of NP cells and chondrocytes, with high expression in CEP chondrocytes during pregnancy and childhood, but its expression decreases with age. Therefore, HSP27 is regarded as an important molecular marker of IDD progression, potentially playing a critical role in cellular protection by aiding cells in coping with degenerative stress induced by mechanical and biological factors. Furthermore, Lambrecht et al. [23] confirmed that HSP27 plays a significant role in maintaining the homeostasis of human articular cartilage cells. However, further research is still required to elucidate the mechanism of action of HSP27 in IDD. Moreover, according to literature reports, the regulation of the HSP27 pathway has been associated with cellular iron transport and ferroptosis [24]. Studies have shown that HSP27 serves as a novel regulatory factor in ferroptosis processes in cancer progression, where its overexpression can protect glioblastoma cells from erastin-induced ferroptosis [25]. Additionally, some studies have indicated that HSP27 restores the antioxidant activity of PRDX1 by interacting with ANXA2, thereby reducing cell apoptosis and ferroptosis, thus preventing severe acute pancreatitis [26]. Therefore, we hypothesize that HSP27 may play a protective role in IDD by slowing down the ferroptosis process in NP cells.

Treating IDD presents challenges due to the lack of effective methods to delay or reverse its pathological progression [27]. Current interventions mainly focus on providing symptomatic relief, including the use of analgesics, anti-inflammatories, and physical therapy [28]. Surgical options such as total disc replacement or spinal fusion surgery are considered as last resorts, albeit with potential intraoperative and postoperative complications [29,30]. Therefore, there is an urgent need to explore new therapeutic strategies aimed at alleviating discogenic pain, promoting IDD regeneration, and restoring IVD tissue balance. In recent years, some small-molecule compounds and peptide drugs have shown promising potential in vitro, in vivo, and clinical studies, providing new possibilities for preventing and treating IDD non-invasively [30–32]. Therefore, this study aims to investigate the expression level of HN in IDD and explore the potential therapeutic effects of HN in the treatment of IDD, while elucidating the specific mechanisms of HN in treating IDD, so as to provide a choice for non-invasive treatment of IDD.

2. Methods

2.1. Collection of human NP specimens

We collected NP specimens from volunteers who underwent spinal surgery. These volunteers were selected based on spinal trauma, idiopathic scoliosis, or disc herniation, while excluding cases of spinal infection, immunosuppression, hypertension, and diabetes. The NP specimens were obtained from 24 volunteers, including 14 males and 10 females, aged between 16 and 72 years. The degree of disc degeneration was assessed using the Pfirrmann grading system. We defined a mild degeneration group (Pfirrmann I-II) consisting of 12 samples from volunteers with idiopathic scoliosis and vertebral fractures, and a severe degeneration group (Pfirrmann IV-V) consisting of 12 samples from different segments of disc herniation. The relevant information for each participant is listed in Supplementary Table S1.

2.2. Culturing and treatment of NP cells

The immortalized human NP cells (0028a) were obtained from Yaji bio-company (http://www.yajimall.com/) and cultured in DMEM/F12 medium (Gibco) supplemented with 15 % fetal bovine serum (Gibco) and 1 % streptomycin/penicillin antibiotics. The cells were incubated at 37 °C with 5 % CO2. Upon reaching confluency, the cells were passaged by trypsinization using 0.25 % Trypsin–EDTA (Gibco) and replanted into 10-cm culture plates at the appropriate density. A ferroptosis cell model was constructed to evaluate the inhibitory effect of HN on NP cells ferroptosis. Erastin was used to induce the ferroptosis phenotype in NP cells. Different concentrations of erastin (2 and 5 μM, HY-15763, MCE) and ferrostatin-1 (Fer-1.2 μM), a commonly used ferroptosis inhibitor (HY-100579, MCE), were added to the cell culture medium for 24 h. The cell survival rate, ROS production and the protein expression levels of ferroptosis markers were analysed. Erastin at 5 μM was found to induce the optimal effect on ferroptosis, and therefore, this concentration was used for subsequent cell treatments. To test its cytotoxicity, different concentrations of HN (20, 50, 100, 200 and 500 Mm, HY-P1928, MCE) were added to the culture medium, and the cell survival rate was analysed. Finally, to investigate the effect of HN on NP cells ferroptosis, different concentrations of HN (25 and 50 μM) were added to the culture medium of cells treated with 5 μM erastin. The ferroptosis markers expression levels and ROS production were analysed after 24 h

of treatment.

2.3. Western blot

Total proteins were extracted from human disc specimens and NP cells using RIPA buffer (Beyotime, China), and the protein concentration was measured by the bicinchoninic acid (BCA) assay (Beyotime, China). Subsequently, proteins were separated by sodium dodecyl sulfate-polyacrylamide gel electrophoresis (SDS-PAGE). Following blocking with 3 % bovine serum albumin, the membranes were incubated with primary antibodies: HN(1:1000, ABIN549044, Antibodies), HSP27 (1:3000, 18284-1-AP, Proteintech), PTGS2(1:1000, ab179800, Abcam), ACSL4(1:2000, YT8070, Immunoway), GPX4 (1:1000, ab125066, Abcam), p-P65(1:2000, YP0191, Immunoway), P65(1:2000, YM3111, Immunoway), MMP13(1:1000, ab39012, Abcam), Col II (1:1000, ab34712, Abcam), TLR9 (1:2000, ab134368, Abcam), JAK1 (1:1000, T57173, Abmart), Phospho-JAK1 (1:1000, TP56310, Abmart), JAK2 (1:1000, T55287, Abmart), Phospho-JAK2 (1:1000, TA3024, Abmart), JAK3(1:1000, T57016, Abmart), Phospho-JAK3 (1:1000, TA8160, Abmart), STAT1(1:1000, T55227, Abmart), Phospho-STAT1(1:1000, T55702, Abmart), STAT2(1:1000, PA6346, Abmart), Phospho-STAT2 (1:1000, TP56499, Abmart), STAT3(1:1000, T55292, Abmart), Phospho-STAT3(1:1000, T56566, Abmart), GAPDH(1:5000, 60004-1-Ig, Proteintech), and β-actin(1:4000, SA00023-4, Proteintech). Subsequently, the membranes were incubated with secondary antibodies: Anti-rabbit IgG (1:5000, SA00013-4, Proteintech) and anti-mouse IgG (1:5000, SA00001-1, Proteintech). Finally, the proteins on the membranes were detected using enhanced chemiluminescence detection reagents (Invitrogen, CA).

2.4. Immunohistochemistry (IHC)

To conduct further analysis, sections from both human and rat discs were collected. After antigen retrieval and blocking with 5 % normal goat serum, the slides were subjected to incubation with primary antibodies, including HSP27(1:200, 18284-1-AP, Proteintech), p-P65 (1:200, YP0191, Immunoway), GPX4(1:100, ab125066, Abcam), ACSL4 (1:200, 22401-1-AP, Proteintech), MMP13(1:100, ab39012, Abcam), Col II (1:100, ab34712, Abcam), p-STAT3(1:100, T56566, Abmart), Rattin(1:200, orb1148108, biorbyt),HN(1:1000, ABIN549044, Antibodies) and secondary antibodies. Subsequently, the sections were treated with DAB solution (Gene-Tech, Shanghai, China) for development and counterstained with hematoxylin. Histological fields were randomly selected in each section and captured at 200× magnification using an Olympus BX63 microscope (Olympus, Japan). The histological fields were observed at a magnification of 200 × using the same microscope. The percentage of positive cells was calculated using Image J software (National Institutes of Health).

2.5. Immunofluorescence staining

NP cells were seeded into flat-bottom 24-well plates at a density of 5 × 10^3 cells per well. Subsequently, they were incubated with 4 % paraformaldehyde, permeabilized with 0.5 % Triton-X 100 in phosphate-buffered saline (PBS) for 10 min, and blocked with PBS containing 1 % BSA. Following this, the cells were subjected to overnight incubation at 4 °C with the appropriate primary antibody. After washing, the cells were then treated with a 1:300 dilution of Alexa Fluor-488 or -594 conjugated anti-rabbit or anti-mouse secondary antibody (Immunoway, USA) for 1 h at room temperature before being imaged using a laser scanning confocal microscope (Olympus, Tokyo, Japan).

2.6. Hematoxylin-eosin (H&E) and safranine-O/fast green staining

The tissue paraffin blocks were sectioned into 4-μm slices for histological evaluation of human samples and rat discs using hematoxylin and eosin (H&E) staining. Moreover, all rats were euthanized 8 weeks post-surgery, and disc tissue sections (5 μm) were prepared and processed as previously described for hematoxylin-eosin (H&E) and Safranin-O/Fast green staining to quantify the degree of IDD. Images were captured using a light microscope.

2.7. Tunel staining

We collected samples from human IVD tissues and rat IDD models, fixing them in 4 % paraformaldehyde and embedding them in paraffin. After sectioning, the samples were deparaffinized and rehydrated, followed by staining with a Tunel staining kit according to the manufacturer's instructions. The disc tissue sections were stained with the Tunel reaction mixture and DAPI. Finally, the sections were observed using a fluorescence microscope, and the proportion of Tunel-positive cells was calculated to assess the apoptosis of NP cells.

2.8. Lentivirus transfection

HSP27 expression was modulated by transfecting LV-HSP27 or LV-shHSP27 (GENE, Shanghai, China) into cells at 30–50 % confluence. Following a 12-h incubation period, cell viability was maintained above 95 %, and the cells were further cultured for an additional three days before being passaged. The efficiency of transfection was assessed using RT-qPCR and western blot analysis.

2.9. Measurement of cytosolic mtDNA

Cytosolic mitochondrial DNA (mtDNA) was assessed using standard PCR subsequent to the specific induction of erastin at predetermined time intervals and concentrations. Initially, half of the cellular specimens underwent lysis employing a mild lysis buffer, while the remaining half were subjected to lysis using a robust lysis buffer. The cell lysates were subjected to cytoplasmic lysis on ice for 20 min employing 0.1 % NP-40, followed by centrifugation at 14,000×*g* for 20 min at 4 °C. Cytosolic mtDNA was isolated from the supernatant cytosolic fraction, while total mtDNA was extracted from the entire cell lysate utilizing the TIANamp Genomic DNA Purification Kit. DNA analysis encompassed standard PCR, agarose gel electrophoresis, and RT-qPCR, as previously outlined, with normalization relative to the mtDNA content within the total cell lysate.

2.10. Assessment of mitochondrial reactive oxygen species (ROS) levels

To gauge mitochondrial ROS levels, MitoSOX (Biosharp) were employed as indicators. Following the treatment, the specimens were stained as per the provided protocols. The fluorescence intensities of MitoSOX were visualized through fluorescence microscopy.

2.11. Cell counting kit-8 (CCK-8) assay

Cell viability was assessed using the Cell Counting Kit-8 (CCK-8) method, following the protocol provided by BD Pharmingen (USA). Cells were seeded in 96-well plates with a volume of 200 μL medium, and the cell density was adjusted to 5 × 10^3 cells per well. To establish a blank control group, 100 μL of culture medium was added to separate wells of the 96-well plates. The plates were then placed in a CO^2 incubator at 37 °C for 24 h to promote optimal cell growth and adherence. After treatment with various concentrations of HN (0, 25, 50, 100, 200 and 500 μM), 10 μL of CCK-8 solution from Kumamoto (Japan) was added to each well. The plates were further incubated for 1 h. Subsequently, the optical density (OD) was measured at 450 nm using a microplate reader (Tecan; Spectra Flour Plus). This procedure was repeated three times, and the average of the collected readings was calculated. The percentage of cell viability was determined using formula (1-mean OD for drug group/mean OD for control group) × 100 %.

2.12. Enzyme-linked immunosorbent assay (ELISA)

Plasma HN levels were quantified using an ELISA kit obtained from Biobyt (orb565009, UK). Following the manufacturer's guidelines, 100 μl of plasma samples were applied to the competitive ELISA plates. The absorbance was subsequently recorded at 450 nm using a microplate reader.

2.13. Measurement of malondialdehyde (MDA), glutathione (GSH), and ferric ion (Fe^{2+})

The levels of GSH, MDA, and Fe^{2+} were quantitatively assessed using commercially available assay kits. GSH levels were determined using a GSH detection kit (Beyotime, S0052, China), while MDA levels were measured with a dedicated MDA assay kit (Beyotime, S0131S, China). The concentration of Fe^{2+} was evaluated using a ferrous ion detection kit (Abcam, ab83366, USA). All assays were performed in accordance with the manufacturer's instructions to ensure accuracy and reliability of the results.

2.14. Assessment of mitochondrial membrane potential (MMP) and mitochondrial permeability transition pore (mPTP) opening

JC-1 assay kit (Beyotime) was employed to measure MMP according to the manufacturer's instructions, followed by analysis via flow cytometry to determine the ratio of JC-1 polymers to monomers. For detection of mPTP opening, the mPTP Assay Kit (Beyotime) was utilized. Treated cells were washed with PBS and subsequently incubated with calcein AM and Co^{2+} quencher at 37 °C for 30 min. After replacing the culture medium, the slides were further incubated at 37 °C for an additional 30 min in the dark. Finally, fluorescence microscopy was utilized to observe the samples.

2.15. Quantitative real-time polymerase chain reaction (real-time qPCR)

To evaluate the effect of HN peptide on mitochondrial transcription, NPCs cells were co-treated with a mitochondrial transcription-specific inhibitor, inositol 4-methyltransferase (IMT1, MCE, HY-134539), and HN peptide for 12 h. Total RNA was extracted using TRIzol reagent (Takara) and converted to cDNA using the Prime Script RT Master Mix (Takara, Japan). Quantitative real-time PCR (qPCR) was performed using the LightCycler 96 (Roche, USA) with SYBR Green I Master Mix (Takara, Japan) to analyze mRNA levels. Gene-specific primers for POSTN and SYBR Premix Ex Taq II (Takara, Japan) were used for amplification on the ABI 7900HT Fast Real-Time PCR System (Applied Biosystems). Relative mRNA expression levels were quantified using the $2^{-\Delta\Delta}$Ct method, and all experiments were performed in triplicate.

2.16. DNA immunoprecipitation

Following treatment, cellular lysis was carried out using a moderate IP buffer (NP-40, Beyotime) supplemented with 1 % protease inhibitors (Beyotime) and 1.5 % phosphatase inhibitor (Beyotime) at 4 °C for 20 min, followed by centrifugation at 14,000×*g* for 15 min at 4 °C to isolate the soluble fraction. The resulting supernatants were then subjected to incubation with anti-dsDNA or IgG isotype control monoclonal antibodies at 4 °C for 8 h, utilizing a protein-to-antibody ratio of 1 mg–5 μg. Subsequently, Protein A/G magnetic beads (MedChemExpress) were co-incubated with the antigen–antibody mixture for 2 h at 4 °C. The beads were then subjected to washing and divided into two portions. One half of the beads was eluted with SDS loading buffer (Boster) and subsequently boiled at 95 °C for 10 min for western blot analysis, while the other half was eluted with chromatin immunoprecipitation (ChIP) elution buffer (5 mM Tris–HCl, 10 mM EDTA, and 1 % SDS). Following proteinase K treatment, DNA extraction was performed using the TIANamp Genomic DNA Kit (TaKaRa), followed by standard PCR analysis as previously described.

2.17. Proximity ligation assay (PLA)

Following treatment, cells were fixed at room temperature for 15 min and subsequently washed twice with PBS. The Duolink® In situ PLA® kit (Sigma–Aldrich) designed for mouse/rabbit samples (with red detection) was employed to visualize the physical interaction between double-stranded DNA (dsDNA) and TLR9, following the provided protocol.

2.18. Establishment of IDD rat model

Prior to aseptic surgery to induce IDD in rats, anesthesia was administered via an injection of pentobarbital sodium (45 mg/kg). Subsequently, prone rats weighing 200–250 g in each group underwent a midline longitudinal incision on the tail, followed by the removal of the left facet joint between the third and fourth lumbar vertebrae to expose the Co7/8 disc. IDD induction was achieved by the insertion of a 30-gauge needle parallel to the endplates, penetrating 3.0 mm into the disc and remaining in situ for 30 s. The control group did not undergo any intervention. Muscle closure was performed using 3-0 silk sutures, while skin margins were sutured with 4-0 nylon sutures. Four weeks post-operation, lumbar H&E staining and Safranin-O/Fast green staining were conducted on the rats.

2.19. Annulus needle puncture and drug treatment

Adult male SD rats weighing 200–250 g (n = 8 per group) were sourced from the Animal Center of Gansu of Sciences, Gansu, China. Following established protocols, the rats were divided into four groups: Sham group, IDD + NS, IDD + HN (0.5 or 1 mg/kg), and IDD + Fer-1. Rats in the IDD + HN group were intraperitoneally injected with 0.5 or 1 mg/kg/day of HN for 56 consecutive days beginning from the day of operation. Rats in the IDD + NS group were intraperitoneally injected with normal saline daily for the same duration. The IDD + Fer-1 group was the positive control group. At 8 weeks post-operation, T2-weighted MRI examinations were conducted to evaluate signal changes in the rats. Furthermore, the degree of disc degeneration was assessed using the Pfirrmann classification.

2.20. Statistical analysis

The group differences were evaluated using one-way analysis of variance (ANOVA) conducted with SPSS software version 19.0 for Windows (IBM, IL, USA). In cases where the ANOVA results indicated statistical significance, pairwise comparisons between the groups were carried out using Bonferroni's post hoc test. The data are expressed as mean ± standard deviation (SD). Statistical significance was defined as p values < 0.05.

3. Results

3.1. The decrease of HN expression in IDD

Based on existing research, HN is linked to various age-related diseases [33], but its expression in IDD has not been reported. To investigate this, we collected IDD tissue samples (n = 6) and rigorously assessed their degenerative status using MRI imaging, H&E staining, and Safranin-O/Fast green staining (Fig. 1A–B). The expression level of MMP13 were also utilized to evaluate the extent of IDD. Of note, tunel staining was conducted to assess the apoptosis of NP cells between the mild and severe degeneration groups ($p < 0.05$, Fig. 1C–D). The results indicated a significantly higher apoptotic rate in the severe degeneration group. Western blot analysis revealed a significant upregulation of MMP13, PTGS2, and ACSL4, along with a downregulation of GPX4 and

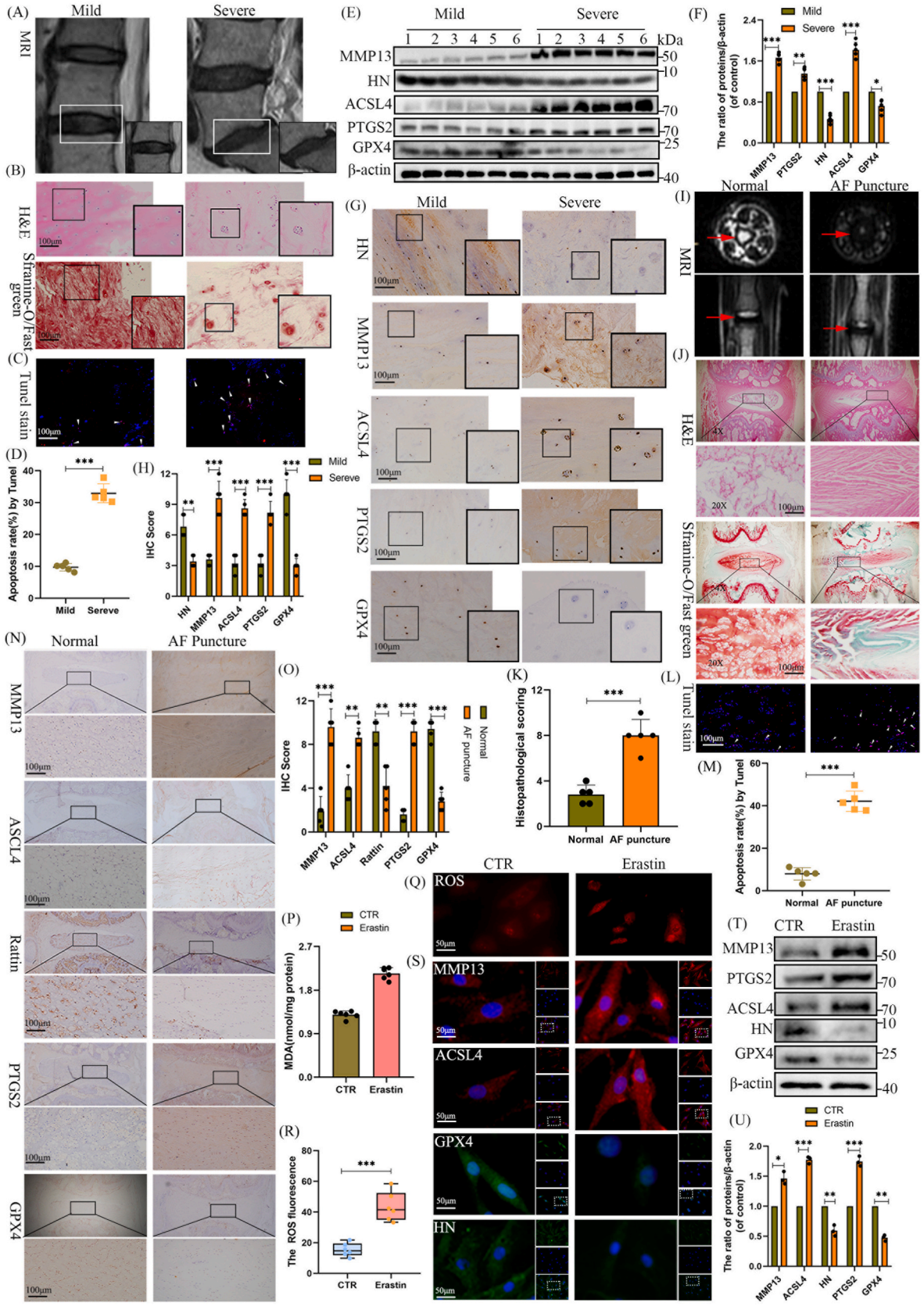

(caption on next page)

Fig. 1. The decrease of HN expression in IDD. (A) MRI images of the spine obtained from patients with varying Pffirmann grades; (B) Histological staining including H&E and Safranine-O/Fast green staining of IVDs derived from patients with different Pffirmann grades (scale bar = 100 μm); (C–D) Tunel staining of IVDs derived from patients with different Pffirmann grades and quantitative analysis (scale bar = 100 μm); (E–F) Western blot of MMP13, PTGS2, HN, ACSL4, and GPX4 and quantitative analysis in various degenerated human discs; (G–H) IHC staining of HN, MMP13, PTGS2, GPX4, and ACSL4 and quantitative analysis (scale bar = 100 μm); (I) MRI images of rat IVDs from normal and AF puncture groups; (J-K)H&E and Safranin-O/Fast green staining of rat IDD models and histopathology score for IDD in the rat model (scale bar = 100 μm); (L–M) Tunel staining of IVDs derived from rats and quantitative analysis; (N–O) IHC staining of Rattin, MMP13, GPX4, PTGS2, and ACSL4 and quantitative analysis (scale bar = 100 μm); (P–R) MDA and ROS detecting of NP cells and quantitative analysis in different groups; (S) Immunofluorescence staining of MMP13, HN, GPX4, and ACSL4 in different groups (scale bar = 50 μm); (T-U)Western blot of MMP13, HN, PTGS2, GPX4, and ACSL4 and quantitative analysis in different groups. *$p < 0.05$, **$p < 0.01$, ***$p < 0.001$ versus Mild or Normal or CTR. The values are presented as the means ± SD from at least three independent experiments.

HN in severely degenerated tissues compared to mildly degenerated tissues ($p < 0.05$, Fig. 1E–F). IHC staining results further confirmed the findings from the western blot analysis ($p < 0.05$, Fig. 1G–H). These findings indicated a reduced expression level of HN in severely degenerated IVD tissues, accompanied by an increase in apoptosis and ferroptosis of NP cells. This suggested that HN may be closely associated with the processes of ferroptosis and apoptosis in NP cells, as well as with the IDD.

To further investigate the relationship between HN expression and ferroptosis in IDD, we established both rat and cellular models of IDD for additional validation. The effectiveness of rat model of IDD was validated through MRI imaging, H&E and Safranin-O/Fast green staining, and histopathological score [34]. MRI results indicated a decreased T2 signal of the IVD in rats post-acupuncture, presenting as "black IVD" syndrome (Fig. 1I). H&E and Safranin-O/Fast green staining showed disrupted AF structure, reduced NP cells and ECM, and severe fibrosis in the model group (Fig. 1J). Histopathological scoring revealed higher scores in the model group compared to the normal group ($p < 0.05$, Fig. 1K), indicating the successful establishment of the IDD model. Tunel staining indicated a significantly higher apoptotic rate in the AF puncture group ($p < 0.05$, Fig. 1L-M). Furthermore, we conducted IHC staining to assess the expression levels of MMP13, PTGS2, and ACSL4, which were found to be elevated, while Rattin expression was decreased in degenerated rat IVDs. The pattern was closely in parallel with the changes in HN expression observed in IDD ($p < 0.05$, Fig. 1N-O).

In addition, we evaluated HN expression in an erastin-induced cellular ferroptosis model. To determine the optimal erastin concentration for inducing ferroptosis in NP cells, we treated NP cells with 1 μM, 2.5 μM, and 5 μM erastin. Western blot results indicated the most significant increase in ACSL4 and PTGS2 expression and the lowest GPX4 expression at 5 μM erastin ($p < 0.05$, Fig. S1A). ROS detection demostrated the highest intracellular ROS fluorescence intensity at 5 μM erastin ($p < 0.05$, Fig. S1B). Subsequently, NP cells were treated with 5 μM erastin at various time points (0 h, 6 h, 12 h, and 24 h). Western blot analysis and ROS detection revealed that ferroptosis marker expression and ROS levels significantly increased after 6 h of treatment, peaking at 12 h. However, this increase did not persist with extended treatment duration ($p < 0.05$, Figs. S1C–D). Consequently, we selected 5 μM erastin to treat NP cells for establishing the ferroptosis cell model. MDA and ROS in NP cells treated with erastin were increased ($p < 0.05$, Fig. 1P-R). Western blot and immunofluorescence assays confirmed the increased expression of MMP13, PTGS2, and ACSL4, along with reduced levels of GPX4 and HN in the ferroptosis cell model ($p < 0.05$, Fig. 1S-U). Overall, our data suggest a potential link between decreased HN expression and cellular ferroptosis, implying its role in the progression of IDD.

3.2. HN treatment induces intracellular expression to alleviate erastin-induced NP cells ferroptosis

In our initial experiments, we demonstrated that ferroptosis in NP cells increased, while HN expression decreased in IDD. This suggested a potential link between reduced HN expression and cellular ferroptosis. Recent studies have indicated that HN significantly increases the protein levels of GPX4 and reduces ROS generation, thereby inhibiting cellular ferroptosis [19]. Therefore, re-expression of HN may represent a promising strategy to inhibit ferroptosis in NP cells and alleviate the progression of IDD. The structure of exogenous HN is illustrated in Fig. 2A. To assess the impact of HN on NP cells, we conducted a CCK-8 assay using concentrations ranging from 0 to 200 μM at various time points (0 h, 6 h, 12 h, 24 h, and 48 h). The results indicated that HN had no significant effect on the cell survival rate, even at the highest concentration of 200 μM ($p < 0.05$, Fig. 2B).

To investigate the effect of exogenous HN on alleviating erastin-induced ferroptosis in NP cells, we treated the cells with varying concentrations of HN (ranging from 0 to 200 μM) in combination with erastin. The viability of NP cells in each group was assessed using the CCK-8 assay. The results showed that NP cell viability decreased following erastin treatment. However, when the concentration of HN was increased to 25 μM, we observed a significant improvement in cell viability, with the most pronounced effect at 50 μM. Notably, further increases in HN concentration did not result in a significant enhancement of cell viability ($p < 0.05$, Fig. S2A). Based on these findings, we have selected 25 μM and 50 μM of HN in regard to subsequent experiments. Fer-1, a ferroptosis inhibitor, was co-treated with erastin as a positive control group. Intracellular concentrations of GSH, MDA, and Fe^{2+} were assessed. The results revealed that a concentration of 25 μM HN effectively reduced the loss of GSH and decreased the levels of Fe^{2+} and MDA. The effects were even more pronounced at 50 μM HN, showing a similar efficacy to that observed in the positive control group ($p < 0.05$, Fig. 2C–E). ROS detection demonstrated that ROS levels in NP cells significantly decreased with HN treatment ($p < 0.05$, Fig. 2F–G). Furthermore, western blot were employed to evaluate cells ferroptosis and ECM metabolism. Results showed that at 25 μM, HN reduced MMP13, ACSL4, and PTGS2 expression while increasing GPX4 and Col II. This effect was further enhanced at 50 μM, indicating the potential of HN to mitigate erastin-induced ferroptosis and induce ECM metabolism in NP cells, thereby alleviating IDD ($p < 0.05$, Fig. 2H–I). Immunofluorescence findings were consistent with western blot analysis ($p < 0.05$, Fig. 2J). Calcein/PI staining also revealed that HN increased survival of NP cells ($p < 0.05$, Fig. S2B).

Although we have confirmed that HN inhibits ferroptosis in NP cells and enhances cell viability, the precise mechanism remains unclear. Previous studies indicated that exogenous HN treatment can stimulate mitochondrial gene expression, thereby preserving mitochondrial function and protecting neurons from Parkinson's disease [35]. We hypothesized that HN may inhibit NP cell ferroptosis by inducing intracellular HN expression. To test this hypothesis, we treated NP cells with varying concentrations of HN (from 0 to 200 μM). Western blot analysis revealed a significant increase in HN expression in NP cells at 25 μM, with the most pronounced effect observed at 50 μM. However, no significant change in intracellular HN expression was noted at 200 μM ($p < 0.05$, see Fig. 2K-L). We subsequently monitored mitochondrial ribosomal RNA (rRNA) transcription levels following HN treatment. Within 3 h, we observed a significant upregulation of various rRNA regions and HN. Although mitochondrial transcript levels slightly declined over time, they remained significantly elevated up to 12 h post-treatment ($p < 0.05$, Fig. 2M). To further validate HN's stimulatory effect on mitochondrial transcription, we employed IMT1, a small molecule inhibitor, to suppress mitochondrial double-stranded RNA (mt-RNA) production. Co-treatment with IMT1 significantly reduced HN

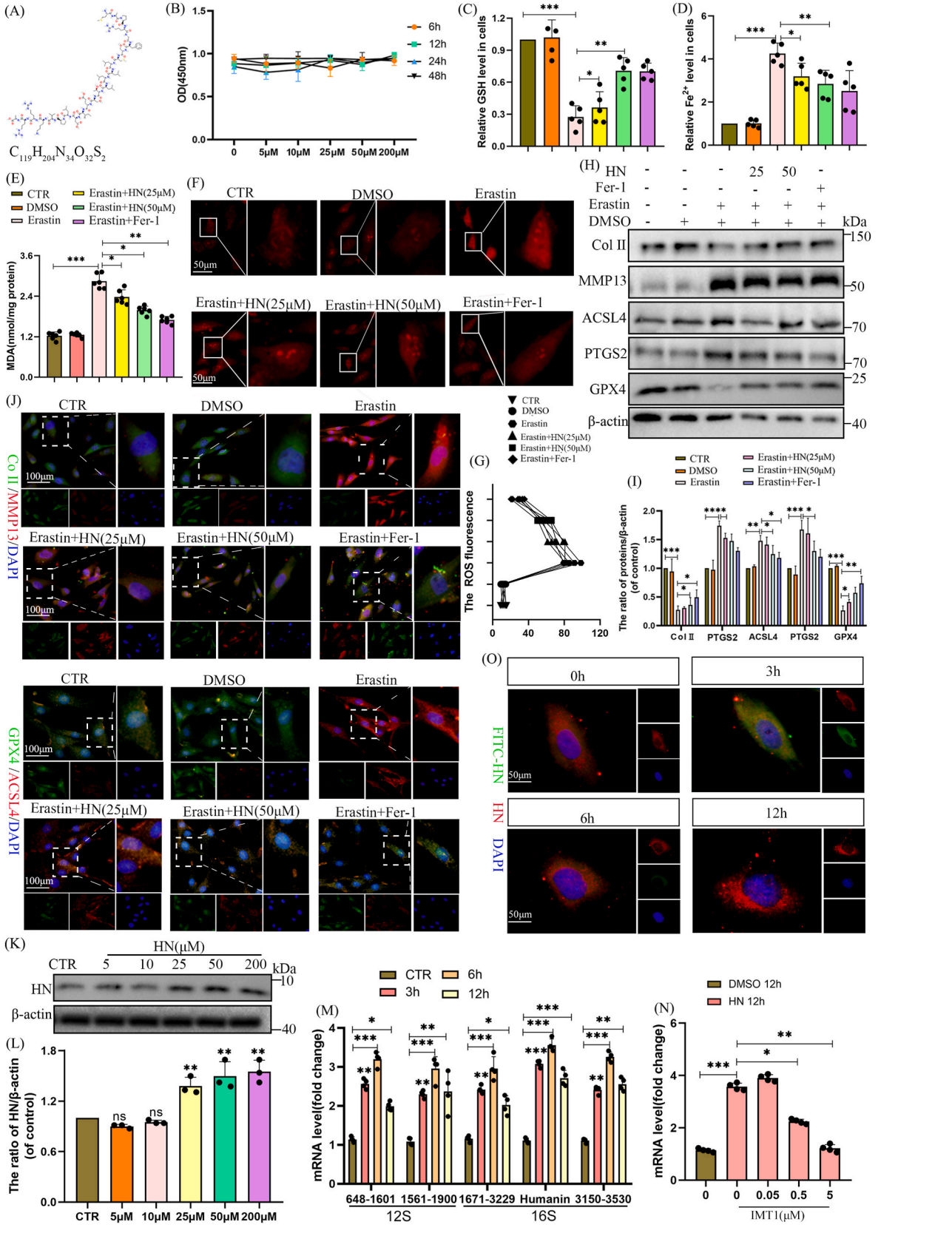

(caption on next page)

Fig. 2. HN treatment induces intracellular HN expression to alleviate erastin-induced NP cells ferroptosis. (A) Molecular structure of HN; (B) Assessment of NP cells viability using the CCK-8 assay after treatment with various concentrations of exogenous HN; (C–E) Measurement of GSH, Fe^{2+}, and MDA levels in NP cells in different experimental groups; (F–G) ROS detecting in NP cells and quantitative analysis in different groups; (H-I)Western blot analysis and quantitative assessment of HN, Col II, MMP13, ACSL4, PTGS2, and GPX4 expression in different experimental groups; (J) Immunofluorescence staining of ACSL4, GPX4, MMP13, and col II (scale bar = 100 μm); (K–L) Western blot analysis and quantitative assessment of intracellular HN when treated with various concentrations of exogenous HN; (M) Real-time qPCR analysis was conducted to amplify different regions of mitochondrial rRNAs, specifically 12S rRNA and 16S rRNA, following HN treatment for designated time periods. Each value on the x-axis corresponds to a specific targeted sequence within the mitochondrial genome; (N) Real-time qPCR analysis by co-treating IMT1 inhibiting mitochondrial gene expression with HN in NP cells; (O) Immunofluorescence of fluorophores conjugated HN (FITC-HN: green) in NP cells for indicated hours. Intracellular HN was stained (red) (scale bar = 50 μm). (M). $^{*}p < 0.05$, $^{**}p < 0.01$, $^{***}p < 0.001$ compared to the control group (CTR). Data are presented as means ± SD from at least three independent experiments.

transcripts induced by HN peptide treatment in a dose-dependent manner ($p < 0.05$, Fig. 2N).

To differentiate between exogenously added HN peptide and intracellular HN, we treated NP cells with FITC-conjugated HN (FITC-HN). As shown in Fig. 2O–a weak HN signal was initially detected in NP cells. After 3 h of FITC-HN treatment, a strong intracellular fluorescence signal was observed, while no signal was detectable after 12 h, indicating peptide degradation. However, cells treated for 12 h exhibited robust intracellular HN signals. These results suggest that exogenous HN treatment not only stimulates mitochondrial gene expression but is also absorbed by cells, ultimately leading to an increased intracellular HN expression.

3.3. *HSP27 may be a target gene regulated by HN and its expression mitigates erastin-induced ferroptosis in NP cells*

We have confirmed that HN can alleviate cellular ferroptosis by inducing itself in expression levels in NP cells. In this process, will HN also affect the expression of other genes? So,we treated NP cells with erastin alone or in combination with HN, with DMSO-treated cells serving as the control group. High-throughput sequencing analysis was subsequently performed to assess the expression of genes. We identified the top 50 DEGs($|\log2\ (FC)| \geq 1$ and $p < 0.05$), visually represented in a heatmap ($p < 0.05$, Fig. 3A). Moreover, multiple sets of volcano plots show the DEGs between the control group and the erastin group, as well as between the erastin and the erastin + HN group ($p < 0.05$, Fig. 3B). Subsequently, genes associated with ferroptosis and IDD were extracted from databases and cross-referenced, revealing MMP2, PTGS2, and HSP27 as commonly DEGs (Fig. 3C). Notably, HSP27 exhibited the most significant alteration, prompting our focus on it ($p < 0.05$, Fig. 3D). Correlation analysis conducted through GEPIA databases revealed a positive association between HN and HSP27 expression ($R = 0.55$, $p < 0.05$), indicating the potential of HN to modulate HSP27 expression to ameliorate ferroptosis ($p < 0.05$, Fig. 3E).

However, the expression of HSP27 in IDD has not been reported, and its relationship with ferroptosis in NP cells is also unclear. So, we examined HSP27 expression in human and rat IDD tissues by western blot and IHC staining, and observed decreased expression in severely degenerated tissues and AF puncture IVD of rat ($p < 0.05$, Fig. 3F–I). In cell model, erastin induced a dose-dependent decrease in HSP27 expression, with significant downregulation at 1 μM and the most pronounced decrease at 5 μM in NP cells ($p < 0.05$, Figs. S3A–B). Time-course analysis revealed a significant reduction in HSP27 expression after 6 h of erastin treatment, however, with the increase of processing time, the expression of HSP27 did not decrease continuously ($p < 0.05$, Figs. S3C–D).

To investigate the relationship between HSP27 and ferroptosis, we performed HSP27 knockdown in NP cells. The outcomes from western blot indicated that HSP27 knockdown led to an increase in the expression of ACSL4, PTGS2, and MMP13, while the expression of GPX4 and Col II decreased in NP cells ($p < 0.05$, Fig. 3J). This suggested that the knockdown of HSP27 may induce ferroptosis and enhance ECM metabolism in NP cells, contributing to their degeneration. Furthermore, we investigated the effects of HSP27 knockdown on cellular ROS levels and mitochondrial function using ROS assays, Mito Tracker Red, and JC-1 staining. The results indicated that, after the inhibition of HSP27 expression, ROS levels in NP cells increased, the number of mitochondria decreased, and mitochondrial membrane potential was altered($p < 0.05$, Fig. 3K-O). We also studied the effects of HSP27 overexpression on ferroptosis, ROS levels, and mitochondrial function, and the efficacy was validated through western blot analysis ($p < 0.05$, Fig. 3P). Western blot results demonstrated that, compared to the erastin-only treated group, the erastin + oe-HSP27 group exhibited reduced expression of MMP13, ACSL4, and PTGS2, along with increased expression of Col II and GPX4 ($p < 0.05$, Fig. 3Q-R). Immunofluorescence staining for MMP13, Col II, GPX4, and ACSL4 corroborated the western blot findings ($p < 0.05$, Fig. S3E). The erastin-mediated increases in ROS levels, decreases in mitochondrial numbers, and imbalances in mitochondrial membrane potential were alleviated following HSP27 overexpression ($p < 0.05$, Fig. 3S–V).

3.4. *HN safeguards NP cells from erastin-induced ferroptosis via increasing HSP27 expression*

In previous studies, we identified HSP27 as a potential target gene regulated by HN and found that HSP27 expression can effectively mitigate erastin-induced ferroptosis in NP cells. To further elucidate whether HN alleviates erastin-induced ferroptosis through the regulation of HSP27 expression, we investigated the regulatory effect of HN on HSP27 expression. Our results demonstrated a significant increase in HSP27 expression starting at 25 μM HN, which plateaued at 50 μM ($p < 0.05$, Fig. 4A-B). Additionally, when examining the impact of HN (50 μM) treatment on HSP27 expression at various time points, we observed an increase in HSP27 expression after 6 hours, which became significantly more pronounced after 12 hours ($p < 0.05$, Fig. 4C-D). IF analysis confirmed that HN treatment resulted in an increased co-expression of HN and HSP27 in NP cells ($p < 0.05$, Fig. 4E).

Subsequently, we explored the necessity of HSP27 expression in HN-mediated alleviation of erastin-induced ferroptosis in NP cells through knockdown and overexpression experiments. Western blot analyses revealed that, compared to the erastin + HN group, the erastin + HN + oe-HSP27 group exhibited decreased expression levels of MMP13, ACSL4, and PTGS2, although the increases in GPX4 and Col II were not statistically significant ($p < 0.05$; Fig. 4F-G). In contrast, in the erastin + HN + shHSP27 group, levels of MMP13, ACSL4, and PTGS2 increased, while levels of GPX4 and Col II decreased compared to the erastin + HN group ($p < 0.05$; Fig. 4H-I). Immunofluorescence staining results further confirmed these western blot findings ($p < 0.05$; Fig. 4J).

Furthermore, we assessed intracellular concentrations of ROS, GSH, MDA, and Fe^{2+}. The results indicated that overexpression of HSP27 and HN treatment reduced GSH depletion, ROS and MDA production, and Fe^{2+} accumulation in the erastin-induced ferroptosis model. However, when HN treatment was accompanied by HSP27 knockdown, GSH consumption in NP cells was not reduced, while ROS and MDA production increased, along with elevated Fe^{2+} levels ($p < 0.05$; Fig. 4K-O). Additionally, Calcein/PI staining was employed to evaluate the survival rate of NP cells across different groups. The results demonstrated that both HN treatment and HSP27 overexpression increased NP cell survival rates, with the highest survival observed during HN treatment in conjunction with HSP27 overexpression. Conversely, when HSP27

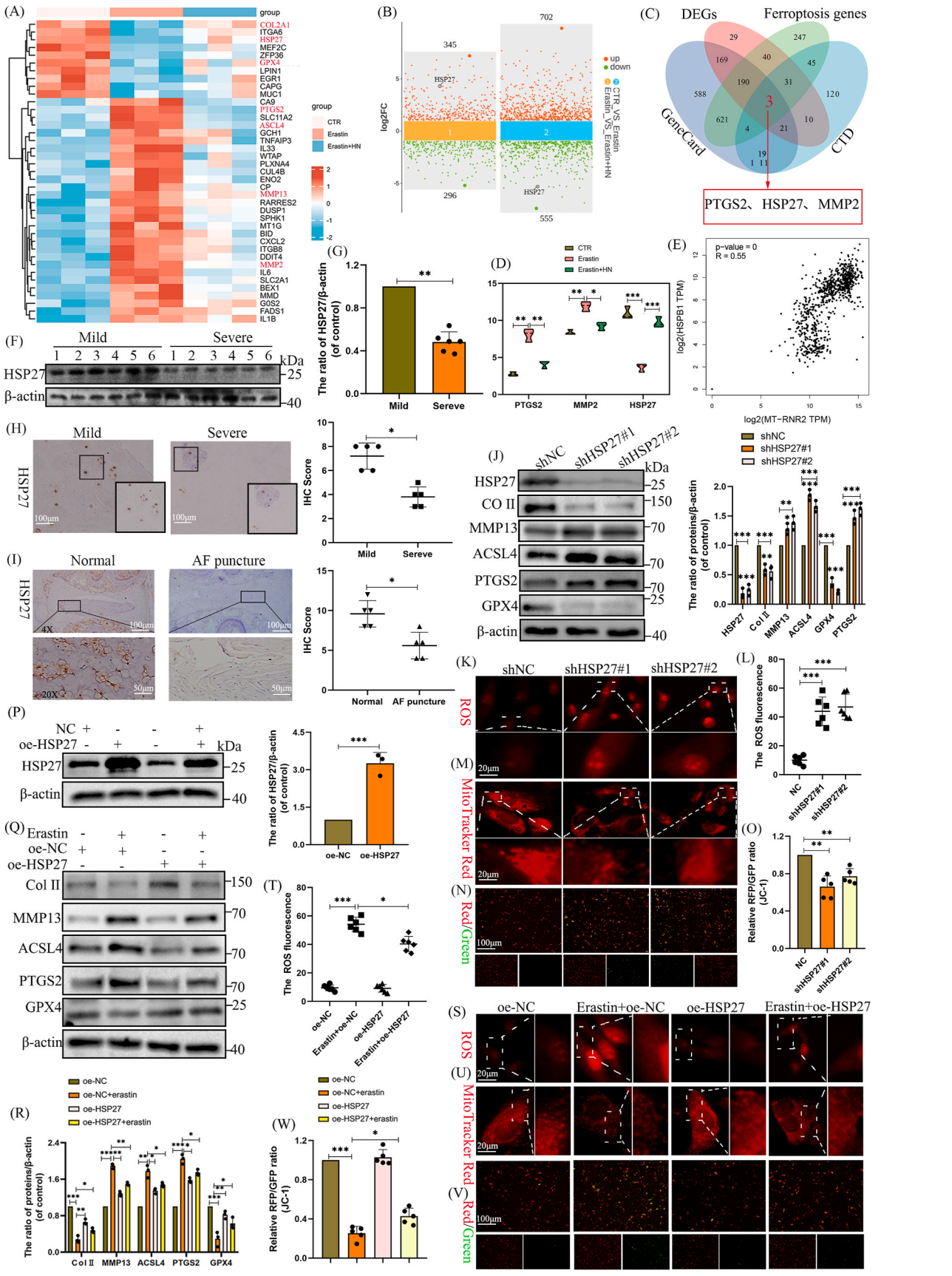

(caption on next page)

Fig. 3. HSP27 may be a target gene regulated by HN and its expression mitigates erastin-induced ferroptosis in NP cells. (A) Heat map showing the top 50 DEGs from transcriptome sequencing results; (B) Volcano plot showing the distribution of DEGs in the transcriptome sequencing results, with green indicating downregulation and red indicating upregulation; (C)Venn diagram of DEGs, ferroptosis related genes from FerrDb database, and IDD-related genes from GeneCards and CTD databases; (D) Violin plot showing the differential expression analysis of MMP2, PTGS2, and HSP27 in three groups; (E) Correlation analysis of HN and HSP27 expression in the GEPIA database ($R = 0.55$, $p < 0.05$); (F–G) Western blot of HSP27 and quantitative analysis in various degenerated human discs; (H–I) IHC staining of HSP27 and quantitative analysis in IVDs from human and rat (scale bar = 100 μm or 50 μm); (J) Western blot of HSP27, ASCL4, MMP13, Col II, PTGS2, and GPX4 and quantitative analysis when HSP27 knockout; (K-L and S-T) ROS detecting in NP cells and quantitative analysis in different groups(scale bar = 20 μm); (M and U) Mito Tracker Red showed the number of mitochondria(scale bar = 20 μm); (V-O and V-W) JC-1 staining and quantitative analysis of MMP in different groups (scale bar = 20 μm).*$p < 0.05$, **$p < 0.01$, ***$p < 0.001$ versus Mild, Normal or NC. The values are presented as the means ± SD from at least three independent experiments.

expression was inhibited, the ability of HN to enhance NP cell survival diminished ($p < 0.05$; Fig. 4P-Q).

Overall, these findings indicate that overexpression of HSP27 enhances the anti-ferroptotic effect of HN, while inhibition of HSP27 expression reduces this effect. This suggested that HN alleviated erastin-induced ferroptosis in NP cells, thereby delaying IDD progression in a manner dependent on HSP27 expression.

3.5. HN mitigates ferroptosis in NP cells by suppressing the NF-κB and JAK2/STAT3 signal pathways

To investigate the mechanisms by which HN expression alleviates ferroptosis in NP cells, we conducted KEGG and GSEA enrichment analyses using genes derived from sequencing data. Our analysis revealed significant enrichment of genes associated with the NF-κB and JAK/STAT signaling pathways ($p < 0.05$; Fig. 5A–B), suggesting that HN may modulate these pathways to mitigate erastin-induced ferroptosis. Previous studies have indicated a close association between the activity of these pathways and ferroptosis [36,37], underscoring their crucial roles in the pathogenesis of IDD [38–40]. Therefore, we focused on these two pathways.

To validate our hypothesis, NP cells were treated with HN (25 and 50 μM) in conjunction with erastin, and the impact on the NF-κB signaling pathway was examined. Western blot analysis showed that HN effectively inhibited the erastin-induced activation of the NF-κB pathway, with a more pronounced effect at higher concentrations ($p < 0.05$; Fig. 5C–D). Immunofluorescence staining further revealed that erastin increased the nuclear translocation of p-P65, while HN partially mitigated this effect ($p < 0.05$; Fig. 5E). Similarly, we explored the influence of HN on the JAK/STAT pathway. Western blot analysis demonstrated that HN significantly inhibited the phosphorylation of JAK2 and STAT3 induced by erastin, without affecting the phosphorylation levels of JAK1, JAK3, STAT1, or STAT2 ($p < 0.05$; Fig. 5F–H). Immunofluorescence staining confirmed that erastin induced increased expression of p-JAK2 and nuclear translocation of p-STAT3, which was partially reduced by HN ($p < 0.05$; Fig. 5I). These results indicated that HN can effectively suppress the activation of both the NF-κB and JAK2/STAT3 signaling pathways induced by erastin.

To further investigate whether HN reduces ferroptosis in NP cells via the NF-κB pathway, we introduced CU-T12-9, an NF-κB pathway agonist, and established four experimental groups: control, erastin, erastin + HN, and erastin + HN + CU-T12-9. Western blot results showed that in the HN + erastin group, the expression levels of MMP13, ACSL4, and PTGS2 decreased, while those of Col II and GPX4 increased compared to the erastin group. This suggested that HN effectively alleviated erastin-induced ferroptosis and degeneration of NP cells. However, in the HN + erastin + CU-T12-9 group, the expression levels of MMP13, ACSL4, and PTGS2 were elevated, while those of Col II and GPX4 were reduced compared to the HN + erastin group, indicating that the protective effect of HN was diminished upon reactivation of the NF-κB pathway ($p < 0.05$; Fig. 5J–K).

Moreover, we investigated the relationship between HN and ferroptosis by introducing Butyzamide, a JAK2/STAT3 pathway agonist. Western blot analyses indicated that the protective effect of HN was weakened upon reactivation of the JAK2/STAT3 pathway, further supporting the conclusion that HN alleviates erastin-induced ferroptosis by inhibiting the JAK2/STAT3 pathway ($p < 0.05$; Fig. 5L-M). Immunofluorescence staining corroborated the western blot results ($p < 0.05$; Fig. 5N). Additionally, we assessed the levels of GSH, MDA, and Fe^{2+} in NP cells across the different treatment groups. The results indicated that HN reduced GSH depletion and lowered MDA and Fe^{2+} levels. However, these effects were reversed upon reactivation of the NF-κB and JAK2/STAT3 pathways with their respective agonists ($p < 0.05$; Fig. 5O-Q). Our findings demonstrate that HN alleviates erastin-induced ferroptosis in NP cells by suppressing the activity of the NF-κB and JAK2/STAT3 signaling pathways.

3.6. HN suppressed NF-κB and JAK2/STAT3 pathway activity and ferroptosis in NP cells depending on HSP27 expression

In previous studies, we demonstrated that HN promotes the expression of HSP27, which alleviated erastin-induced ferroptosis in NP cells. We also identified that this effect of HN is mediated, at least in part, by the inhibition of the NF-κB and JAK2/STAT3 signaling pathways. Existing literature confirmed that HSP27 expression could inhibit the activity of the NF-κB pathway [41] and was closely associated with the activity of the JAK2/STAT3 pathway [42]. Therefore, we hypothesized that HN might inhibit the activity of these two pathways, at least partly, through the regulation of HSP27 expression.

To test this hypothesis, we investigated the impact of HSP27 knockdown on the activity of the NF-κB and JAK2/STAT3 pathways. Western blot analysis revealed that HSP27 knockdown resulted in increased expression of p-JAK2, p-STAT3, and p-P65 ($p < 0.05$; Fig. 6A–B). Additionally, immunofluorescence staining showed that the nuclear translocation of p-STAT3 and p-P65 was enhanced following HSP27 knockdown, indicating increased activity of the NF-κB and JAK2/STAT3 pathways ($p < 0.05$; Fig. 6C–D). To further investigate whether HN's inhibition of the NF-κB and JAK2/STAT3 pathways is dependent on HSP27 regulation, we established four experimental groups: control, erastin, erastin + HN, and erastin + HN + shHSP27. Western blot results indicated that, compared to the erastin + HN group, the expression levels of p-JAK2, p-STAT3, and p-P65 in the erastin + HN + shHSP27 groups were elevated, yet lower than those observed in the erastin group. This suggested that the ability of HN to inhibit NF-κB and JAK2/STAT3 pathway activity was partially diminished following HSP27 knockdown ($p < 0.05$; Fig. 6E–H). Furthermore, immunofluorescence results confirmed the findings from the Western blot analysis ($p < 0.05$; Fig. 6I).

Moreover, we continued to explore whether HN's inhibition of erastin-induced ferroptosis in NP cells is dependent on HSP27 expression. Western blot and immunofluorescence analyses revealed increased expressions of MMP13, ACSL4, and PTGS2, alongside decreased levels of GPX4 and Col II in the shHSP27 + erastin + HN group compared to the erastin + HN group. This indicated that the ability of HN to mitigate erastin-mediated ferroptosis in NP cells was compromised when HSP27 expression was inhibited ($p < 0.05$; Fig. 6J-L). Additionally, the levels of ROS and MDA in NP cells were measured, revealing that the production of ROS and MDA was not decreased upon HSP27 expression inhibition ($p < 0.05$; Fig. 6M–O). Calcein/PI staining further confirmed that HN enhanced the survival of NP cells; however, this protective effect was

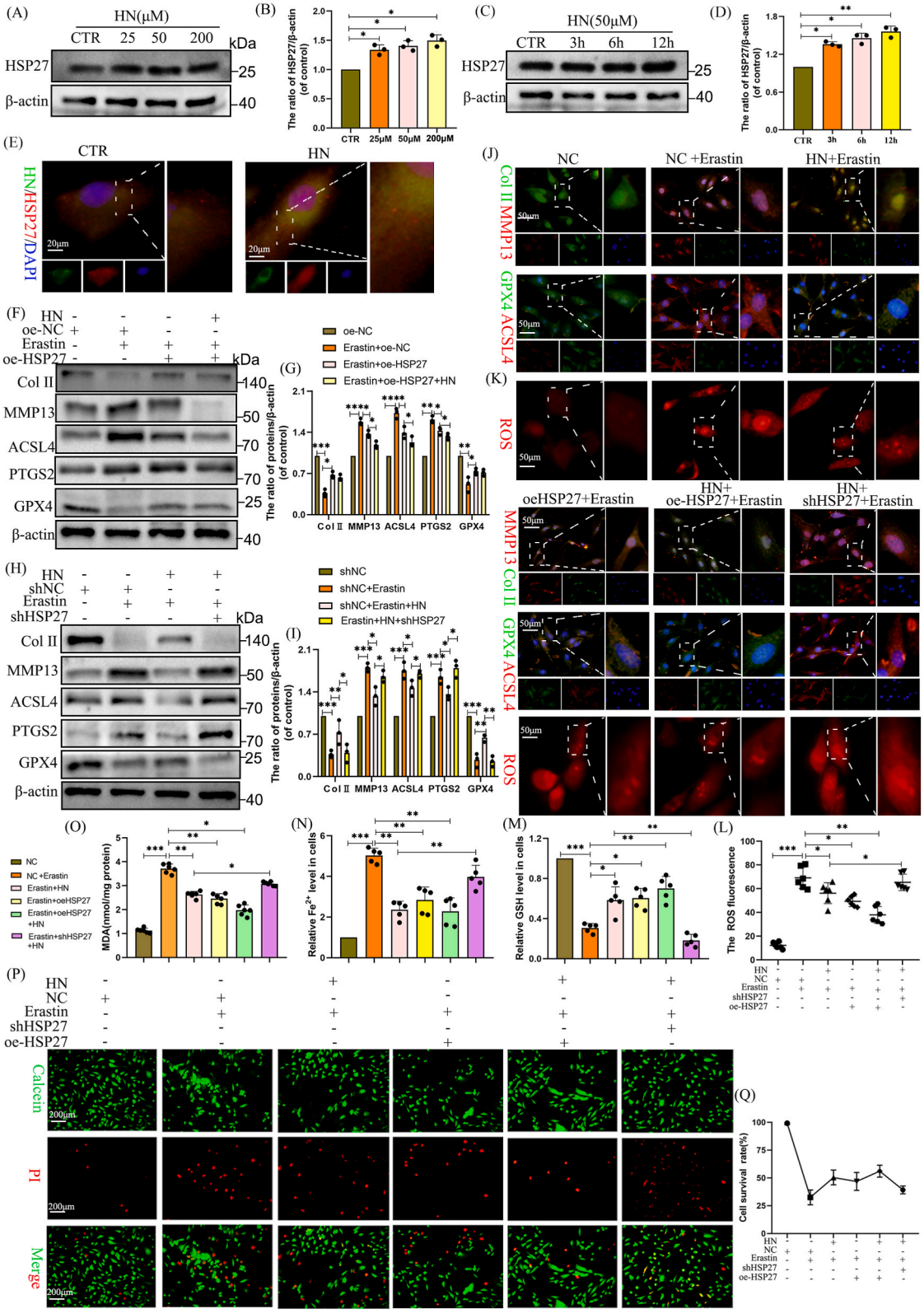

Fig. 4. HN safeguards NP cells from erastin-induced ferroptosis via increasing HSP27 expression. (A-D and F-I) Western blot analysis of PTGS2, ACSL4, GPX4, MMP13, HSP27, and Col II and quantitative assessment in various experimental groups; (E and J) Immunofluorescence staining of MMP13, Col II, GPX4, HSP27, HN, and ACSL4 and quantitative analysis across different groups (scale bar = 50 μm); (K-L) ROS detecting in NP cells and quantitative analysis in different groups(scale bar = 50 μm); (M) Quantification of GSH levels in NP cells among different experimental groups; (N) Quantification of Fe^{2+} levels in NP cells among different experimental groups; (O) Quantification of MDA levels in NP cells among different experimental groups; (P-Q) Calcein/PI staining of NP cells in different experimental groups (scale bar = 200 μm). $*p < 0.05$, $**p < 0.01$, $***p < 0.001$ versus CTR or NC. The values are presented as the means ± SD from at least three independent experiments.

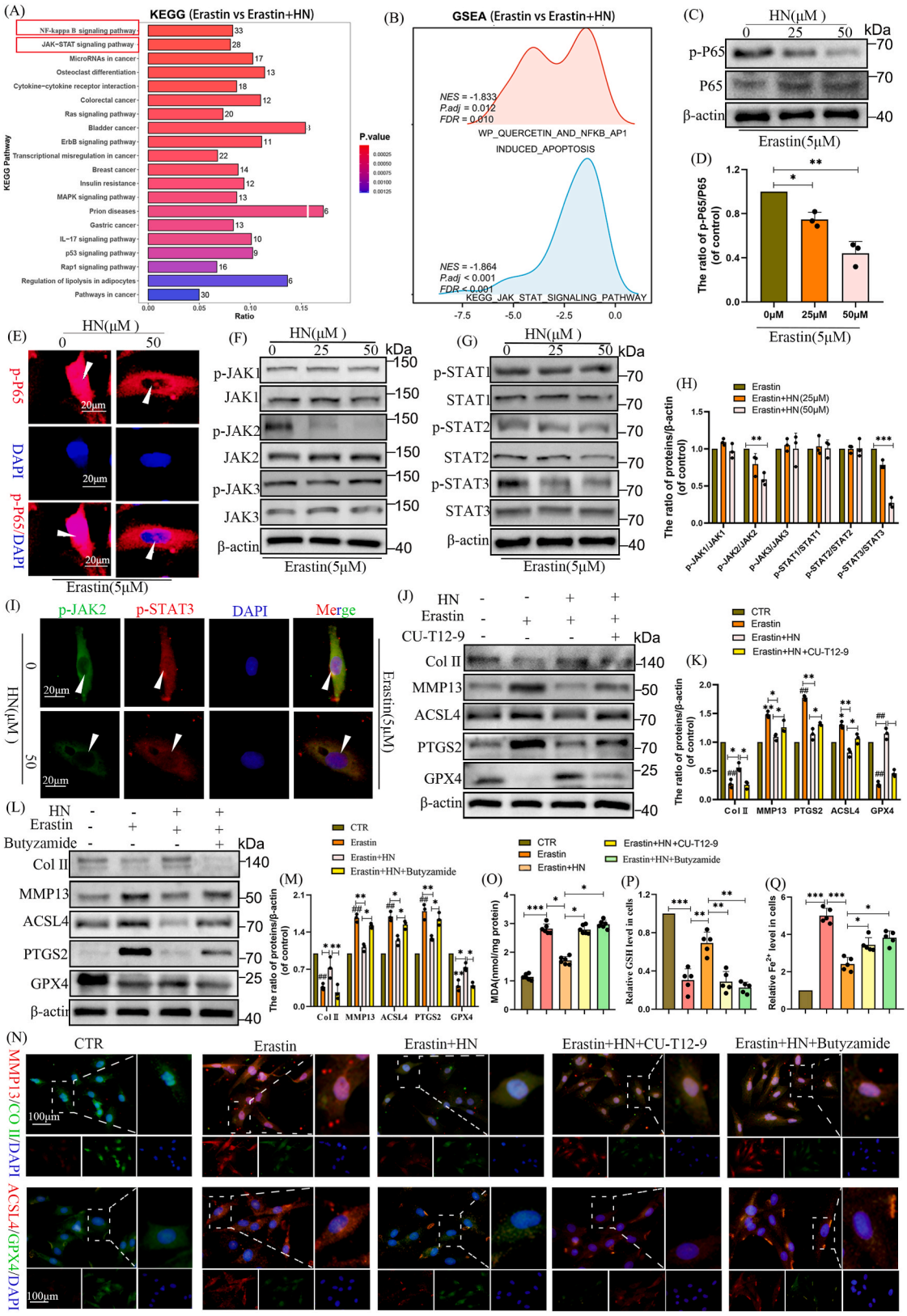

Fig. 5. HN mitigates ferroptosis in NP cells by suppressing the NF-κB and JAK2/STAT3 signal pathways. (A) KEGG enrichment analysis of DEGs(Erastin VS Erastin + HN); (B) GSEA enrichment analysis of genes; (C-D, F-G, J-K, and L-M) Western blot of PTGS2, p-P65, P65, ACSL4, GPX4, MMP13, JAK1/2/3, STAT1/2/3, p-JAK1/2/3, p-STAT1/2/3, and Col II and quantitative analysis in different groups; (E,I and N) Immunofluorescence staining of Col II, MMP13, ACSL4, GPX4, p-JAK2, p-STAT3, and p-P65 in different groups (,scale bar = 20 μm or 100 μm); (O–Q) Measurement of GSH, Fe^{2+}, and MDA levels in NP cells in different experimental groups. *$p < 0.05$, **$p < 0.01$, ***$p < 0.001$ versus CTR. The values are presented as the means ± SD from at least three independent experiments.

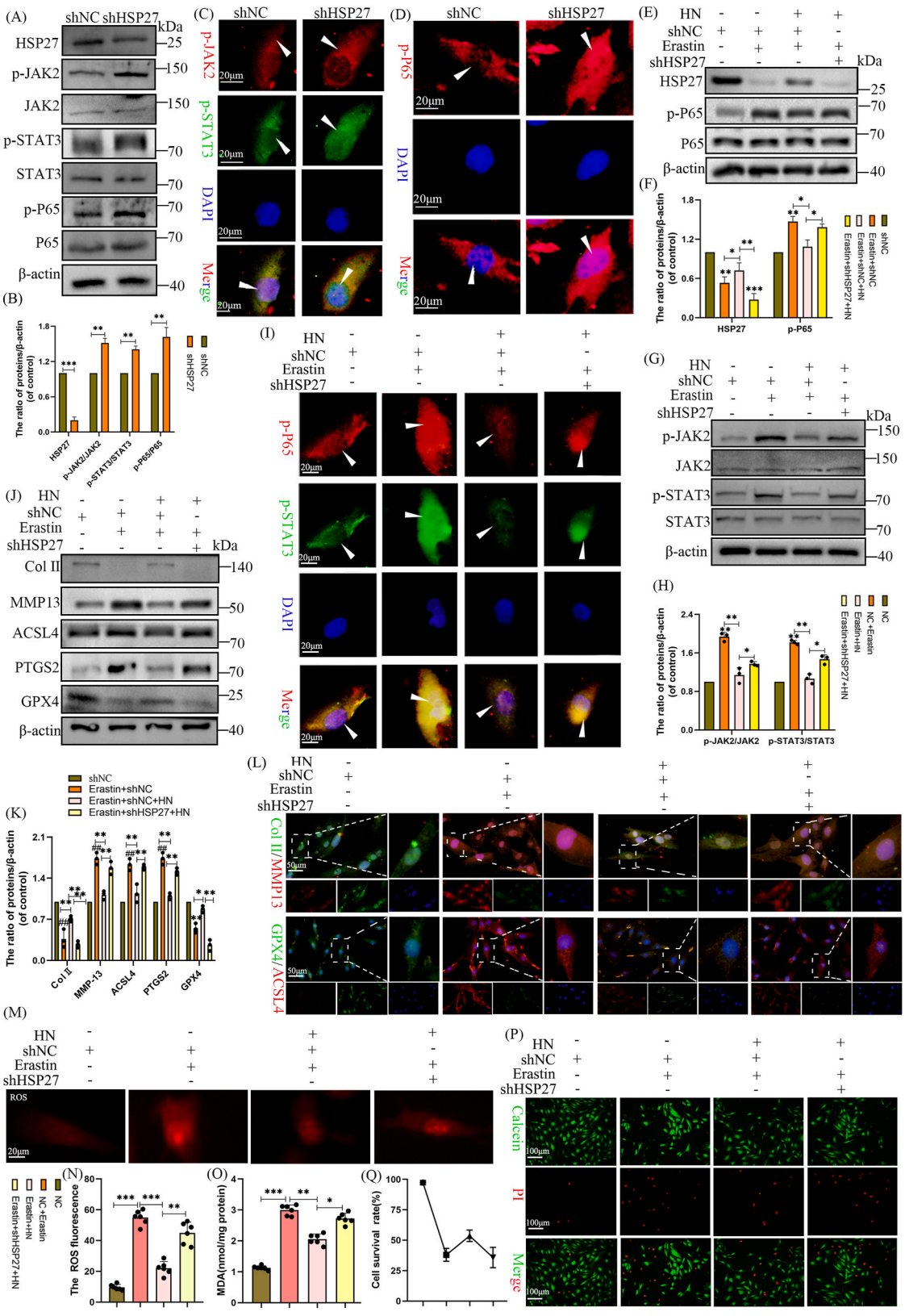

Fig. 6. HN suppresses ferroptosis in NP cells and activity of NF-κB and JAK2/STAT3 pathways depend on HSP27 expression partially. (A–B) Western blot of p-JAK2, JAK2, p-STAT3, STAT3, P65, and p-P65 and quantitative analysis when HSP27 was knocked down; (C–D) Immunofluorescence staining of p-JAK2, p-STAT3, and p-P65 when HSP27 was knocked down; (E-H and J-K)Western blot of HSP27, p-JAK2,JAK2, p-STAT3, STAT3, p-P65, P65, GPX4 PTGS2, MMP13, Col II, and ACSL4 in different groups; (I and L) Immunofluorescence staining of p-STAT3, p-P65, GPX4, MMP13, Col II, and ACSL4 in different groups (scale bar = 50 or 20 μm); (M−N) ROS detecting in NP cells and quantitative analysis in different groups(scale bar = 20 μm); (O) MDA level in NP cells in different groups; (P–Q) Calcein/PI staining of NP cells in different experimental groups (scale bar = 100 μm).*$p < 0.05$, **$p < 0.01$, ***$p < 0.001$ versus shNC. The values are presented as the means ± SD from at least three independent experiments.

diminished when HSP27 expression was inhibited ($p < 0.05$; Fig. 6P-Q).

In conclusion, these findings suggested that the suppression of HSP27 expression attenuated HN's ability to inhibit the NF-κB and JAK2/STAT3 pathways, thereby reducing its efficacy in alleviating erastin-induced ferroptosis in NP cells. HN inhibited the activity of the NF-κB and JAK2/STAT3 pathways and alleviated cell ferroptosis, partially dependent on HSP27 expression.

3.7. HN maintains mitochondrial homeostasis to prevent mtDNA leakage-induced TLR9 activation, thereby reducing NF-κB pathway activation

HN is a polypeptide secreted by mitochondria, and its main function is to maintain mitochondrial homeostasis [35]. According to existing studies, an imbalance in mitochondrial homeostasis in NP cells could lead to an increased opening of the mPTP gate, resulting in the extravasation of mtDNA into the cytoplasm. Once in the cytoplasm, mtDNA bind to TLR9, thereby activating the downstream NF-κB pathway and mediating corresponding biological effects [43,44]. Therefore, we speculated that HN inhibited the NF-κB pathway not only by regulating HSP27, but also by maintaining mitochondrial homeostasis and reducing mtDNA extravasation binding to TLR9, thereby inhibiting the activation of the downstream NF-κB pathway.

To investigate the impact of HN on NP cells mitochondria, we initially assessed the effects of different concentrations of erastin on mitochondrial homeostasis. Through diverse assays, such as Cancein AM + Co^{2+} for mPTP opening, JC-1 staining for MMP changes, and MitoSOX Red staining for mtROS levels, we observed a dose-dependent increase in mPTP opening, MMP, and mtROS production upon erastin treatment ($p < 0.05$, Fig. 7A–E). Furthermore, we used TOMM20-labeled mitochondria and double-stranded DNA for fluorescence colocalization. The results showed that with an increase of erastin concentration, the number of mitochondria decreased and the mtDNA extravasated into the cytoplasm increased ($p < 0.05$, Fig. 7J). Additionally, erastin treatment significantly increased TLR9 expression detected by western blot and cytoplasmic leakage of mitochondrial DNA (mtDNA)-ND1 demonstrated by agarose gel electrophoresis and immunofluorescence ($p < 0.05$, Fig. 7F–I). The DNA IP and PLA assays confirmed a direct ND1-TLR9 interaction, which strengthened with rising erastin concentration ($p < 0.05$, Fig. 7K-M).

Subsequently, we assessed how different concentrations of HN affected erastin-induced mitochondrial dysfunction. CsA, an mPTP inhibitor, was used as a positive control group after co-treatment with erastin. Notably, at 25uM and 50uM concentrations, HN effectively reduced mPTP opening, mitigated MMP changes, and decreased mtROS production induced by erastin. Furthermore, the fluorescence co-localization of TOMM20-labeled mitochondria and mtDNA showed that after 25uM and 50uM treatment, the number of mitochondria was more than that in erastin group, but less mtDNA was exfiltrated into the cytoplasm ($p < 0.05$, Fig. 7N-Q, S, and U). In addition, we investigated whether HN could inhibit TLR9 activity and attenuate mtDNA binding to TLR9. Western blot results showed that after HN treatment with different concentrations, TLR9 expression decreased, which was consistent with that after CsA treatment ($p < 0.05$, Fig. 7R and T). Our DNA IP and PLA results demonstrated that HN decreased the interaction between erastin-induced dsDNA and TLR9, similar to the positive control group (CsA + Erastin) ($p < 0.05$, Fig. 7V and W-X).

Thus, we concluded that HN diminished mtROS production, maintained mitochondrial membrane potential, reduced mPTP opening, limited mtDNA leakage into the cytoplasm, and attenuated the binding between mtDNA and TLR9, thereby alleviating erastin-induced ferroptosis in NP cells.

3.8. HN alleviates IDD by inhibiting NP cells ferroptosis in rats

Using the above mentioned methodology, we induced an IDD model in rats through AF needle puncture, followed by an evaluation of the therapeutic potential of HN in this model. Specifically, a 26G needle was employed to puncture the IVDs of the rats. The control group was none treatment, while the model group underwent intraperitoneal injection administration of either normal saline (NS) or varying doses of HN (0.5 or 1 mg/kg) in conjunction with Fer-1, which was designated as the positive control. The complete experimental procedure is depicted in Fig. 8A. To assess the absorption of HN administered via intraperitoneal injection in rats, we measured the plasma concentration of HN using ELISA. The results revealed a significant increase in HN levels in the plasma 15 min post-treatment with HN (0.5 or 1 mg/kg), peaking at 30 min. However, after an hour, the serum concentration of HN had remarkably decreased, although it remained elevated compared to the control group, indicating a potential degradation of HN ($p < 0.05$, as illustrated in Fig. 8B). Furthermore, considering that IVD is an avascular structure, with the nutrition of its NP cells primarily sourced from the CEP, we aimed to investigate whether the administered HN could penetrate into the IVD. To achieve this, we administered FITC-labeled HN via intraperitoneal injection and subsequently examined the expression pattern of FITC-HN in the IVD after 30 min. The results indicated that FITC-HN was present not only in the CEP but also within the NP cells, as depicted in Fig. 8C.

At eight weeks post-surgery, MRI analysis was utilized to precisely quantify the water content of the IVDs, a critical diagnostic parameter for IDD. The MRI imaging results showed a significant decrease in T2 signal intensity of the rat IVD and a reduction in intervertebral space in the IDD + NS group compared to the sham surgery group. Conversely, both the HN treatment group and the Fer-1 treatment group showed a significant increase in T2 signal intensity of the NP tissue in the rat IVD compared to the IDD + NS group (Fig. 8D). Moreover, the evaluation of IDD degree through H&E staining and Safranin-O/Fast green staining revealed a significant decrease in NP size and a noticeable increase in AF irregularity in the puncture group compared to the sham surgery group, indicating severe IDD. Remarkably, utilizing treatment with HN and Fer-1 significantly improved these degenerative changes (Fig. 8E). Histopathological score, based on MRI, H&E staining, and Safranin-O/Fast green staining results, quantitatively assessed the severity of IDD. The NS treatment group showed higher scores than the sham surgery group, whereas after treatment with HN and Fer-1, the scores were significantly lower than those in the NS treatment group ($p < 0.05$, Fig. 8F).

Additionally, we utilized immunofluorescence to assess the expression levels of GPX4, Col II, MMP13, and ACSL4, whereas IHC staining was employed to evaluate the expression levels of p-P65, p-STAT3, Rattin, and HSP27. The IHC staining results are noteworthy, showing a significant reduction in the expression of p-STAT3 and p-P65 and increase of HSP27 and Rattin in both the HN and Fer-1 treatment groups compared to the puncture plus NS group ($p < 0.05$, Fig. 8G–H). Immunofluorescence results demonstrated increased expressions of ASCL4 and MMP13 in the degeneration group, but decreased expression in the HN treatment group and positive control group. In contrast, GPX4 and Col II exhibited the opposite trend ($p < 0.05$, Fig. 8I).

These findings confirmed that both HN and Fer-1 effectively inhibit IDD. Therefore, it could be concluded that HN provided a protective effect against IDD induced by needle puncture (Fig. 9).

4. Discussion

IDD is a common spinal condition characterized by the structural and functional deterioration of the IVD in the lumbar spine [4]. Various factors such as aging, injury, and immune responses contribute to structural alterations in the IVD, encompassing diminished disc height, apoptosis of NP cells, AF rupture, calcification of CEP, and imbalance in the ECM metabolism, with a specific emphasis on the compromised function and decreased population of NP cells within the IVD [5,6]. It is widely recognized that the depletion of NP cells induced by ferroptosis plays an essential role in initiating and accelerating the progression of IDD [8,45,46]. Currently, treatment strategies for IDD mainly focus on

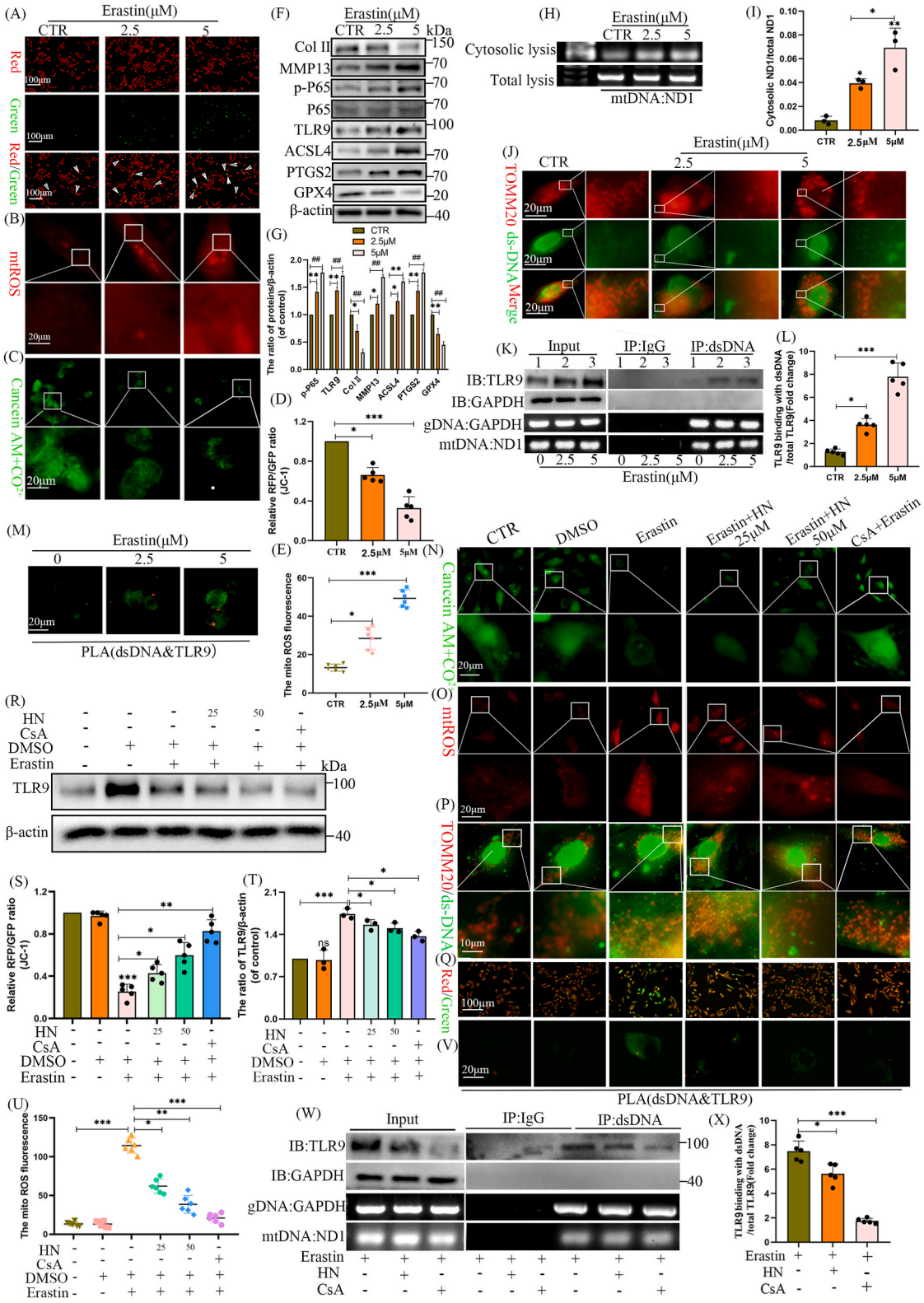

Fig. 7. HN maintains mitochondrial homeostasis to prevent mtDNA leakage-induced TLR9 activation, thereby reducing NF-κB pathway activation. (A, D Q, and S) JC-1 staining and quantitative analysis of MMP in different groups (scale bar = 100 μm); (B, E, O, and U) MitoSOX red staining and quantitative analysis in different groups (scale bar = 20 μm). (C and N)Representative fluorescence images of calcein AM/Co^{2+} quencher staining in different groups; (F, G, R, and T) Western blot of PTGS2, p-P65, ACSL4, GPX4, MMP13, TLR9, and Col II and quantitative analysis in different groups; (H–I) DNA agar gelatin electrophoresis images of mtDNA (ND1) in cytosolic or total lysates of NP cells and quantitative analysis in different groups. (J and P) Immunofluorescence staining of dsDNA and TOMM20 in different groups (original magnification 40×, scale bar = 20 μm); (K-L and W-X) Representative DNA immunoprecipitation images and quantification of the enrichment level of TLR9 in the DNA immunoprecipitates in different groups. (M and V) The physical interaction between dsDNA and TLR9 from in situ PLA images of NP cells in different groups.*$p < 0.05$, **$p < 0.01$, ***$p < 0.001$ versus CTR. The values are presented as the means ± SD from at least three independent experiments.

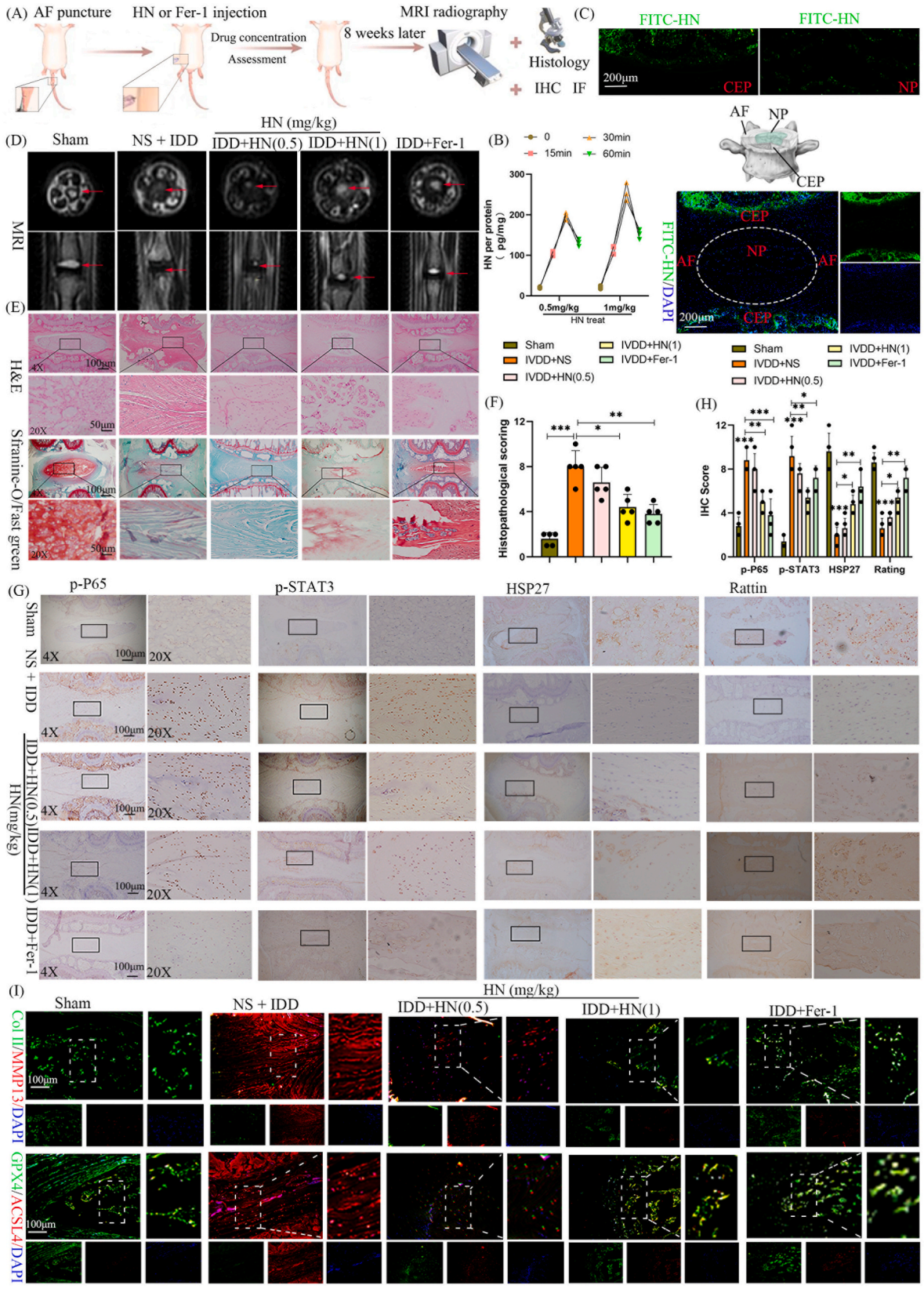

Fig. 8. HN alleviates IDD by inhibiting NP cells ferroptosis in rats. (A) The experimental procedure conducted in vivo; (B) ELISA for detecting FITC-HN In rat serum at the indicated time points; (C) Within 30 min after intranasal treatment, FITC-HN was detected associated with the IVD; (D–E) MRI images, H&E, and Safranin-O/fast green staining of rat discs in different groups (scale bar = 100 μm); (F) Histopathological score were utilized to assess the extent of IDD in different groups; (G–H) IHC staining of p-STAT3, p-P65, HSP27,and Rattin and quantitative analysis in different groups(scale bar = 100 μm); (I) Immunofluorescence of GPX4, ACSL4, Col II, and MMP13 in different groups (scale bar = 100 μm). $^{*}p < 0.05$, $^{**}p < 0.01$, $^{***}p < 0.001$ versus Sham or NS + IDD. Values are presented as the mean ± SD from at least three independent experiments.

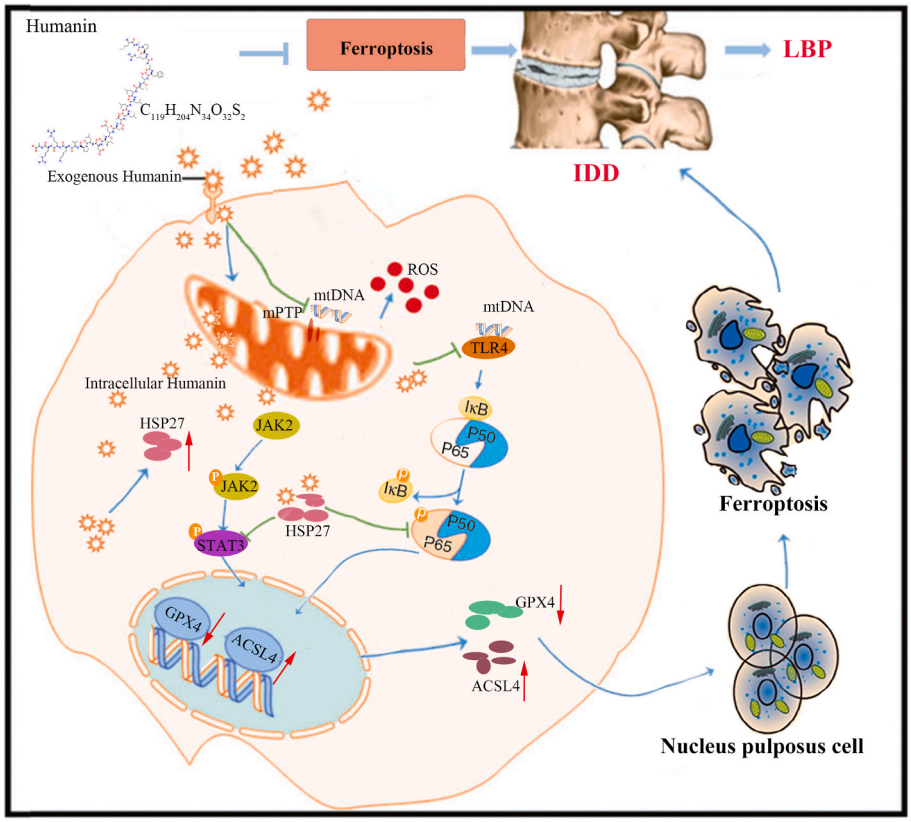

Fig. 9. Proposed schematic representation of how HN reduces ferroptosis in NP cells to alleviate IDD.

alleviating symptoms, including the use of analgesics, anti-inflammatories, and physical therapy, while surgical interventions are generally considered a last resort [29]. HN and its derivative have the capability to diminish oxidative stress, mitigate mitochondrial dysfunction, decrease levels of ROS, and demonstrate anti-inflammatory, antioxidant, and anti-apoptotic properties across various organs [16,17]. Furthermore, HN notably attenuated the decline in cellular viability and generation of ROS, while markedly augmenting the protein expression of GPX4, a pivotal regulatory protein in the process of ferroptosis [19]. However, the expression of HN in IDD and its potential protective effects on NP cells remain unclear and warrant further investigation.

In this study, we conducted a novel analysis of HN expression, termed "rattin" in rodents, in human and rodent IVD tissues. Of note, our findings revealed downregulation of HN and rattin expression in NP tissues of IDD-afflicted subjects compared to healthy IVDs, suggesting their potential involvement in IDD regulation. Subsequently, we investigated the pharmacological effects of exogenous HN in cellular and rodent models of IDD. Our cellular experiments demonstrated that HN effectively attenuated erastin-induced ferroptosis in NP cells by increasing intracellular HN expression. This is in consistent with the study of Kim et al., who also found that exogenous HN can regulate the expression of intracellular HN to delay the progression of Alzheimer's disease [35]. Erastin-induced ferroptosis primarily occurs through inhibition of the Xc system, resulting in glutathione depletion, Fe^{2+} accumulation, oxidative stress, and mitochondrial dysfunction, ultimately leading to cell ferroptosis [7]. Additionally, animal experiments further confirmed the therapeutic potential of HN, as treatment with HN alleviated the progression of needle-induced IDD in rats. This indicates that exogenous HN may ameliorate IDD conditions by inhibiting ferroptosis in NP cells. These findings are in consistent with recent research demonstrating the ability of HN to alleviate intrauterine adhesions by inhibiting ferroptosis in endometrial epithelial cells [47].

To delve into the other molecular mechanisms underlying the reduction of ferroptosis in NP cells by HN, we conducted high-throughput sequencing on NP cells treated with erastin and (or) HN. The group treated solely without erastin and HN served as the control. Differential gene expression analysis was performed, intersecting the identified genes with those related to IDD and ferroptosis, ultimately pinpointing the target gene: HSP27. Concurrently, we investigated the relationship between HSP27 and IDD through human IDD tissue specimens, cellular models, and animal IDD models. Similarly, our results revealed a decreased expression of HSP27 in degenerated IVD compared to normal ones, consistent with findings by Tsuneaki et al. [22]. Additionally, Lambrecht et al. [23] conducted differential expression analysis on normal and osteoarthritis-afflicted chondrocytes, observing reduced HSP27 expression in osteoarthritis chondrocytes and positing its crucial role in maintaining the homeostasis of human articular cartilage cells. Li et al. [48] discovered that Thrombospondin-1 upregulates HSP27 to enhance the autophagy level of chondrocytes, thereby delaying the progression of osteoarthritis. These result suggested a close association between HSP27 and the pathological process of IDD. However, whether the expression of HSP27 in NP cells is related to cell ferroptosis has not been reported and elucidated. Thus, we explored for the first time the effect of HSP27 on NP cells ferroptosis, revealing that knockdown of HSP27 increases ferroptosis in NP cells, while overexpression of HSP27 mitigates erastin-induced cells ferroptosis. Based on existing research, erastin is a specific inducer of ferroptosis, inhibiting HSP27 expression through the heat shock factor 1-dependent pathway in cancer cells [24]. Knockdown of HSP27 enhances erastin-induced ferroptosis, whereas overexpression of HSP27 inhibits it. Hence, HSP27 acts as a negative regulator of ferroptosis in cancer cells [25,26,49], consistent with our findings.

Additionally, this study found that inhibiting HSP27 expression leads to an increase in ROS levels in NP cells, thereby impairing mitochondrial function. Existing literature indicates that HSP27 can reduce ROS

production, effectively preventing oxidative stress damage in cardiac H9c2 cells, and this protective mechanism is closely related to the activation of the Akt signaling pathway, which further enhances cell survival [50,51]. Furthermore, research has shown that the absence of HSP27 disrupts mitochondrial function and induces lethal autophagy (mitophagy), a process that depends on the activity of CerS1 [52]. SQSTM1/P62 promotes lysophagy via formation of liquid-like condensates maintained by HSP27 [53]. Therefore, HSP27 plays a crucial role in protecting cells from oxidative stress, maintaining mitochondrial function, and promoting cell survival, which is consistent with our research findings.

Subsequently, we performed KEGG and GSEA enrichment analysis and observed significant enrichment in the NF-κB and JAK/STAT pathways. Existing research indicates that there is a close association between the activity of the NF-κB and JAK/STAT pathways and ferroptosis [36,37], playing crucial roles in the pathogenesis of IDD [38–40]. In this study, we discovered that HN significantly alleviated erastin-induced ferroptosis in NP cells by suppressing the NF-κB and JAK2/STAT3 signal pathway. This finding echoes the results from research in cerebrovascular diseases, where HN also reduced the production of cytokines such as TNF-α, IL-1β, and IL-6 through NF-κB inhibition, exerting neuroprotective and anti-inflammatory effects [54]. Furthermore, in other studies on acute lung injury, HN demonstrated its ability to suppress the NF-κB pathway, leading to a decrease in the number of total cells and neutrophils in bronchoalveolar lavage fluid from mice, as well as reduced secretion of inflammatory cytokines and levels of ROS and MDA [55]. In a recent study, carried out by Thapak et al. [56] observed that treatment with HN reduced the levels of pro-inflammatory and chemotactic cytokines in the plasma of traumatic brain injury animals while reduced gp-130 and p-STAT3 levels in the hippocampus. In addition, HN has been shown to prevent a pro-inflammatory environment in various neurological diseases such as Alzheimer's disease, stroke, aging, and metabolic disease [57,58].

Notably, research has also revealed that the activation of the JAK2/STAT3 signaling pathway by HN results in increased expression of SH3 domain-binding protein 5, which plays a vital role in anti-cell death activity in neural cells [59]. Additionally, studies have indicated that HN can reactivate the JAK2/STAT3 signaling pathway through the PI3K/AKT pathway, exhibiting neuroprotective effects in stroke patients, hinting at the promising potential of HN as a stroke therapeutic agent [60]. These experimental results are inconsistent with our findings. This may be due to the fact that they are different mechanisms of action of JAK2/STAT3 pathways in different diseases. For example, some studies have pointed out that the activation of JAK2/STAT3 pathways can stimulate the production of matrix-degrading factors such as PTGS2 and MMP13 in NP cells, thereby accelerating the progression of IDD [61,62]. However, there are also studies suggesting that the activation of the JAK2/STAT3 pathway can promote cell proliferation and thus inhibit cells ferroptosis [63,64].

In the current study, we also found out that the inhibition of the NF-κB pathway, JAK2/STAT3 pathway, and ferroptosis in NP cells by HN is partially dependent on the expression of HSP27. We conducted knockdown experiments of HSP27 in NP cells. The experimental results revealed that knocking down HSP27 led to an increase in p-P65 nuclear translocation and a decrease in p-STAT3 nuclear translocation. Moreover, upon the addition of HN to NP cells of shHSP27, we observed a decrease ability of HN to inhibit p-P65 and p-STAT3 nuclear translocation induced by erastin. Similarly, after inhibiting the expression of HSP27, we continued to explore the effect of HN on erastin-mediated ferroptosis in NP cells, and found that the ability of HN to alleviate erastin-induced ferroptosis in NP cells also reduced. In a study by Wang et al. [65], it was confirmed that specific HSP27 deficiency in cardiomyocytes exacerbates post-infarction cardiac dysfunction through NF-κB-mediated leukocyte recruitment. Sims et al. [66] found imatinib prevents intrinsic resistance by promoting doxorubicin-mediated NF-κB/p65 nuclear localization and repression of NF-κB targets in a STAT3-dependent manner, and by preventing activation of a novel STAT3/HSP27/p38/Akt survival pathway. Furthermore, the regulation of the HSP27 pathway has been associated with cellular iron transport and ferroptosis [24]. Lambrecht et al. [23] confirmed that HSP27 plays a significant role in maintaining the homeostasis of human articular cartilage cells. Some studies have shown that HSP27 serves as a novel regulatory factor in ferroptosis processes in cancer, where its overexpression can protect glioblastoma cells from erastin-induced ferroptosis [25]. Other studies have indicated that HSP27 restores the antioxidant activity of PRDX1 by interacting with ANXA2, thereby reducing cell apoptosis and ferroptosis, thus preventing severe acute pancreatitis [26]. These studies align with our findings, further supporting the significant role of HSP27 in regulating NF-κB pathway, JAK2/STAT3 pathway, and ferroptosis in NP cells. This discovery provides a new perspective for our understanding of the pathogenesis of IDD and theoretical support for potential therapeutic strategies.

In our study, we further discovered that HN can maintain the mitochondrial membrane potential of NP cells and reduce the production of mtROS, thereby preserving mitochondrial homeostasis and effectively alleviating erastin-induced ferroptosis in NP cells. Furthermore, we observed that HN not only maintains the steady state of mPTP and reduces the extrusion of mtDNA but also inhibits the expression of TLR9, thereby reducing the binding of mtDNA to TLR9. Research has shown that external harmful stimuli can lead to decreased mitochondrial membrane potential, opening of the mitochondrial permeability transition pore, and release of mtDNA into the cytoplasm [67]. mtDNA, as a circular DNA fragment containing unmethylated CpG, can be recognized by pattern recognition receptors and induce the activation of damage-associated molecular patterns [68]. Previous studies have confirmed that the extrusion of mtDNA into the cytoplasm can bind to cGAS and TLR9, thereby mediating the pyroptosis of NP cells [43,44]. In this study, we unexpectedly found that the binding of mtDNA to TLR9 was significantly reduced after treatment with HN. There have been studies to confirm that HN can improve ovalbumin-induced asthmatic airway inflammation by inhibiting the expression of TLR4 [69] and has been observed to acutely reverse the upregulation of TLR4 in mice with acute lung injury [55].

Multiple risk factors, including mechanical overload, inflammation, and nutritional deficiency, can disrupt mitochondrial homeostasis, which is closely associated with the development of IDD [70]. When mitochondria are damaged, their normal functions are interfered with, leading to increased production of ROS, disruption of calcium ion balance, and leakage of key substances such as cytochrome C and apoptosis-inducing factors. These pathophysiological phenomena are considered crucial factors in the loss of NP cells function and the progression of IDD [71]. HN, as a small peptide, exhibits remarkable abilities in maintaining mitochondrial homeostasis. It plays a significant protective role within cells by inhibiting the permeability transition of mitochondrial membranes, reducing ROS production, preserving the integrity of mitochondrial DNA, and suppressing mitochondrial-related apoptotic pathways [33,72,73]. This provides important clues and hints for our deep understanding of the mechanism of HN in alleviating erastin-induced ferroptosis in NP cells and offers a new and reliable option for drug therapy for IDD.

In the treatment of IDD, drug-loaded biomaterials are emerging as a cutting-edge research direction. These materials not only provide structural support but also facilitate targeted therapy by controlling drug release, thereby improving the biological environment of the IVD and effectively slowing disease progression [74]. Currently, common drug-loaded biomaterials include hydrogels, polymer microspheres, and nanoparticles. Research has demonstrated that S14G-humanin was incorporated into lactoferrin (Lf-POS) to develop a novel brain drug delivery system based on self-assembled poly(ethylene glycol)-poly(D, L-lactic-co-glycolic acid) (PEG-PLGA) polymersomes conjugated with Lf-POS [75]. This innovative system holds promise as a brain-targeting peptide drug delivery platform for intravenous administration, thus

providing long-lasting neuroprotective effects. Additionally, loading HN onto nanoparticles has been shown to reduce age-related macular degeneration. This drug delivery system's capacity to decrease retinal cell apoptosis, along with its favorable pharmacokinetics and biocompatibility, makes it a promising option for the treatment of age-related macular degeneration [76]. So, incorporating HN into bioactive materials such as hydrogels and nanoparticles can substantially improve its stability and bioactivity, thereby enhancing its potential application in the treatment of IDD. This approach offers new ideas and strategies for addressing IDD, warranting further exploration in future research.

However, this study still has several limitations. Firstly, the currently used animal models of IDD have difficulties in fully simulating the complex physiological environment of human IDD. But the acupuncture-induced rat IDD model is a relatively classical model and has been widely used in the study of IDD [77]. Secondly, during the establishment of the puncture IDD model, human factors may introduce trauma, affecting the accuracy of the experimental results. Despite the existence of various IDD animal models, there is still no ideal model that can fully simulate the biomechanical environment of human IDD. Finally, although we collected both degenerated and non-degenerated IVD tissues from human IVD samples (n = 12) and evaluated the expression of HN and HSP27 using IHC staining and western blot techniques, the conclusions drawn are still subject to further validation by large-scale studies due to the limited sample size. Despite the above limitations, this study still reveals a novel mechanism of HSP27 in the development of IDD and confirms that HN can regulate the expression of HSP27 to inhibit ferroptosis and thereby slow down the progression of IDD. Although HN still has a long way in clinical application, this discovery undoubtedly opens a new avenue for the treatment of IDD.

5. Conclusion

This study reports for the first time that the expression level of HN is reduced in IDD. Exogenous HN treatment can induce intracellular HN expression, which not only inhibits the NF-κB and JAK2/STAT3 pathway but also upregulates the expression of HSP27 to reduce ferroptosis in NP cells. Furthermore, Exogenous HN treatment maintains the mitochondrial homeostasis of NP cells to prevent mtDNA leakage-induced TLR9 activation, thereby reducing NF-κB pathway activation and ferroptosis in NP cells. Therefore, HN has the potential to become a promising drug for the treatment of IDD.

Author contributions

Daxue Zhu: Conceptualization, Methodology, Software, and Writing Original draft preparation, Zhaoheng Wang, Yanhu Li, Shijie Chen: Data curation, Visualization, Investigation, and Software, Xuewen Kang: Supervision, Editing, and Validation, All the authors above approved the version of the manuscript to be published.

Ethics approval and consent to participate

All experimental designs and protocols involving animals and human samples were approved by the Animal Ethics Committee (approval D2023-172) and Medical Ethics Committee of Lanzhou University Second Hospital, Gansu, People's Republic of China (approval 2023A-161) and complied with the recommendations of the academy's animal research guidelines. And the human specimens involved in this study have obtained the informed consent of the patients.

Declaration of competing interest

The authors declare that they have no financial or personal relationships with other people or organizations that could inappropriately influence or bias the work reported in this paper. Additionally, the authors have no conflicts of interest to disclose.

Acknowledgements

We are indebted to colleagues from Lanzhou University Second Hospital. We are grateful to all the patients who agree to provide samples of NP in the study. This work was supported by National Natural Science Foundation of China (82272536 and 82460436), and Natural Science Foundation of Gansu Province (23JRRA1012).

Appendix A. Supplementary data

Supplementary data to this article can be found online at https://doi.org/10.1016/j.jot.2024.12.002.

References

[1] Zhu D, Zhang G, Guo X, Wang Y, Liu M, Kang X. A new hope in spinal degenerative diseases: piezo1. BioMed Res Int 2021;2021:6645193. https://doi.org/10.1155/2021/6645193.
[2] Hall JA, Konstantinou K, Lewis M, Oppong R, Ogollah R, Jowett S. Systematic review of decision analytic modelling in economic evaluations of low back pain and sciatica. Appl Health Econ Health Policy 2019;17:467–91. https://doi.org/10.1007/s40258-019-00471-w.
[3] GdaIIaP Collaborators. Global, regional, and national incidence, prevalence, and years lived with disability for 328 diseases and injuries for 195 countries, 1990-2016: a systematic analysis for the Global Burden of Disease Study 2016. Lancet 2017;390:1211–59. https://doi.org/10.1016/S0140-6736(17)32154-2.
[4] Moore RJ. The vertebral endplate: disc degeneration, disc regeneration. Eur Spine J 2006;15(Suppl 3):S333–7.
[5] Ding F, Shao Z-w, Xiong L-m. Cell death in intervertebral disc degeneration. Apoptosis : an international journal on programmed cell death 2013;18:777–85. https://doi.org/10.1007/s10495-013-0839-1.
[6] Molladavoodi S, McMorran J, Gregory D. Mechanobiology of annulus fibrosus and nucleus pulposus cells in intervertebral discs. Cell Tissue Res 2020;379:429–44. https://doi.org/10.1007/s00441-019-03136-1.
[7] Dixon SJ, Lemberg KM, Lamprecht MR, Skouta R, Zaitsev EM, Gleason CE, et al. Ferroptosis: an iron-dependent form of nonapoptotic cell death. Cell 2012;149:1060–72. https://doi.org/10.1016/j.cell.2012.03.042.
[8] Fan C, Chu G, Yu Z, Ji Z, Kong F, Yao L, et al. The role of ferroptosis in intervertebral disc degeneration. Front Cell Dev Biol 2023;11:1219840. https://doi.org/10.3389/fcell.2023.1219840.
[9] Wang W, Jing X, Du T, Ren J, Liu X, Chen F, et al. Iron overload promotes intervertebral disc degeneration via inducing oxidative stress and ferroptosis in endplate chondrocytes. Free Radic Biol Med 2022;190:234–46. https://doi.org/10.1016/j.freeradbiomed.2022.08.018.
[10] Miller B, Kim SJ, Kumagai H, Yen K, Cohen P. Mitochondria-derived peptides in aging and healthspan. J Clin Invest 2022;132. https://doi.org/10.1172/jci158449.
[11] Sreekumar PG, Kannan R. Mechanisms of protection of retinal pigment epithelial cells from oxidant injury by humanin and other mitochondrial-derived peptides: implications for age-related macular degeneration. Redox Biol 2020;37. https://doi.org/10.1016/j.redox.2020.101663.
[12] Yang H, Cui Y, Tang Y, Tang X, Yu X, Zhou J, et al. Cytoprotective role of humanin in lens epithelial cell oxidative stress-induced injury. Mol Med Rep 2020;22:1467–79. https://doi.org/10.3892/mmr.2020.11202.
[13] Caricasole A, Bruno V, Cappuccio I, Melchiorri D, Copani A, Nicoletti F. A novel rat gene encoding a Humanin-like peptide endowed with broad neuroprotective activity. FASEB Journal : Official Publication of the Federation of American Societies For Experimental Biology 2002;16:1331–3.
[14] Yen K, Wan J, Mehta HH, Miller B, Christensen A, Levine ME, et al. Humanin prevents age-related cognitive decline in mice and is associated with improved cognitive age in humans. Sci Rep 2018;8:14212. https://doi.org/10.1038/s41598-018-32616-7.
[15] Cai H, Liu Y, Men H, Zheng Y. Protective mechanism of humanin against oxidative stress in aging-related cardiovascular diseases. Front Endocrinol 2021;12. https://doi.org/10.3389/fendo.2021.683151.
[16] Hazafa A, Batool A, Ahmad S, Amjad M, Chaudhry SN, Asad J, et al. Humanin: a mitochondrial-derived peptide in the treatment of apoptosis-related diseases. Life Sci 2021;264:118679. https://doi.org/10.1016/j.lfs.2020.118679.
[17] Lue Y, Swerdloff R, Jia Y, Wang C. The emerging role of mitochondrial derived peptide humanin in the testis. Biochim Biophys Acta Gen Subj 2021;1865:130009. https://doi.org/10.1016/j.bbagen.2021.130009.
[18] Celvin B, Zaman F, Aulin C, Sävendahl L. Humanin prevents undesired apoptosis of chondrocytes without interfering with the anti-inflammatory effect of dexamethasone in collagen-induced arthritis. Clin Exp Rheumatol 2020;38:129–35.
[19] Zou L, Huang J, Zhang Q, Mo H, Xia W, Zhu C, et al. The humanin analogue (HNG) alleviates intrauterine adhesions by inhibiting endometrial epithelial cells ferroptosis: a rat model-based study. Human Reproduction (Oxford, England) 2023;38:2422–32. https://doi.org/10.1093/humrep/dead196.
[20] Kampinga HH, Garrido C. HSPBs: small proteins with big implications in human disease. Int J Biochem Cell Biol 2012;44:1706–10. https://doi.org/10.1016/j.biocel.2012.06.005.

[21] Carra S, Alberti S, Arrigo PA, Benesch JL, Benjamin IJ, Boelens W, et al. The growing world of small heat shock proteins: from structure to functions. Cell Stress Chaperones 2017;22:601–11. https://doi.org/10.1007/s12192-017-0787-8.
[22] Takao T, Iwaki T. A comparative study of localization of heat shock protein 27 and heat shock protein 72 in the developmental and degenerative intervertebral discs. Spine 2002;27:361–8.
[23] Lambrecht S, Dhaenens M, Almqvist F, Verdonk P, Verbruggen G, Deforce D, et al. Proteome characterization of human articular chondrocytes leads to novel insights in the function of small heat-shock proteins in chondrocyte homeostasis. Osteoarthritis Cartilage 2010;18:440–6. https://doi.org/10.1016/j.joca.2009.10.008.
[24] Sun X, Ou Z, Xie M, Kang R, Fan Y, Niu X, et al. HSPB1 as a novel regulator of ferroptotic cancer cell death. Oncogene 2015;34:5617–25. https://doi.org/10.1038/onc.2015.32.
[25] Yuan F, Sun Q, Zhang S, Ye L, Xu Y, Xu Z, et al. HSP27 protects against ferroptosis of glioblastoma cells. Hum Cell 2022;35:238–49. https://doi.org/10.1007/s13577-021-00645-6.
[26] He J, Hou X, Wu J, Wang K, Qi X, Wei Z, et al. Hspb1 protects against severe acute pancreatitis by attenuating apoptosis and ferroptosis via interacting with Anxa2 to restore the antioxidative activity of Prdx1. Int J Biol Sci 2024;20:1707–28. https://doi.org/10.7150/ijbs.84494.
[27] Vadalà G, Russo F, Di Martino A, Denaro V. Intervertebral disc regeneration: from the degenerative cascade to molecular therapy and tissue engineering. J Tissue Eng Regen Med 2015;9:679–90. https://doi.org/10.1002/term.1719.
[28] Mohd Isa IL, Teoh SL, Mohd Nor NH, Mokhtar SA. Discogenic low back pain: anatomy, pathophysiology and treatments of intervertebral disc degeneration. Int J Mol Sci 2022;24. https://doi.org/10.3390/ijms24010208.
[29] Zhang X-B, Hu Y-C, Cheng P, Zhou H-Y, Chen X-Y, Wu D, et al. Targeted therapy for intervertebral disc degeneration: inhibiting apoptosis is a promising treatment strategy. Int J Med Sci 2021;18:2799–813. https://doi.org/10.7150/ijms.59171.
[30] Kamali A, Ziadlou R, Lang G, Pfannkuche J, Cui S, Li Z, et al. Small molecule-based treatment approaches for intervertebral disc degeneration: current options and future directions. Theranostics 2021;11:27–47. https://doi.org/10.7150/thno.48987.
[31] Kim JW, Jeon N, Shin DE, Lee SY, Kim M, Han DH, et al. Regeneration in spinal disease: therapeutic role of hypoxia-inducible factor-1 alpha in regeneration of degenerative intervertebral disc. Int J Mol Sci 2021;22. https://doi.org/10.3390/ijms22105281.
[32] Yang F, Liu W, Huang Y, Yang S, Shao Z, Cai X, et al. Regulated cell death: implications for intervertebral disc degeneration and therapy. Journal of orthopaedic translation 2022;37:163–72. https://doi.org/10.1016/j.jot.2022.10.009.
[33] Kong BS, Lee C, Cho YM. Mitochondrial-encoded peptide MOTS-c, diabetes, and aging-related diseases. Diabetes & metabolism journal 2023;47:315–24. https://doi.org/10.4093/dmj.2022.0333.
[34] Lai A, Gansau J, Gullbrand SE, Crowley J, Cunha C, Dudli S, et al. Development of a standardized histopathology scoring system for intervertebral disc degeneration in rat models: an initiative of the ORS spine section. JOR Spine 2021;4:e1150. https://doi.org/10.1002/jsp2.1150.
[35] Kim KH. Intranasal delivery of mitochondrial protein humanin rescues cell death and promotes mitochondrial function in Parkinson's disease. Theranostics 2023;13:3330–45. https://doi.org/10.7150/thno.84165.
[36] Zhu J, Sun R, Yan C, Sun K, Gao L, Zheng B, et al. Hesperidin mitigates oxidative stress-induced ferroptosis in nucleus pulposus cells via Nrf2/NF-κB axis to protect intervertebral disc from degeneration. Cell Cycle 2023;22:1196–214. https://doi.org/10.1080/15384101.2023.2200291.
[37] Zhao Y, Wang C, Yang T, Wang H, Zhao S, Sun N, et al. Chlorogenic acid alleviates chronic stress-induced duodenal ferroptosis via the inhibition of the IL-6/JAK2/STAT3 signaling pathway in rats. J Agric Food Chem 2022;70:4353–61. https://doi.org/10.1021/acs.jafc.2c01196.
[38] Suzuki S, Fujita N, Fujii T, Watanabe K, Yagi M, Tsuji T, et al. Potential involvement of the IL-6/JAK/STAT3 pathway in the pathogenesis of intervertebral disc degeneration. Spine 2017;42:E817–24. https://doi.org/10.1097/BRS.0000000000001982.
[39] Bai X, Jiang M, Wang J, Yang S, Liu Z, Zhang H, et al. Cyanidin attenuates the apoptosis of rat nucleus pulposus cells and the degeneration of intervertebral disc via the JAK2/STAT3 signal pathway in vitro and in vivo. Pharm Biol 2022;60:427–36. https://doi.org/10.1080/13880209.2022.2035773.
[40] Wu J, Chen Y, Liao Z, Liu H, Zhang S, Zhong D, et al. Self-amplifying loop of NF-kappaB and periostin initiated by PIEZO1 accelerates mechano-induced senescence of nucleus pulposus cells and intervertebral disc degeneration. Mol Ther 2022. https://doi.org/10.1016/j.ymthe.2022.05.021.
[41] Saraswati SSK, Rana AK, Singh A, Anang V, Singh A, Natarajan K. HSP-27 and HSP-70 negatively regulate protective defence responses from macrophages during mycobacterial infection. Microbes Infect 2023;25:105126. https://doi.org/10.1016/j.micinf.2023.105126.
[42] Zhang Xl, Zhang Xy, Ge Xq, Liu Mx. Mangiferin prevents hepatocyte epithelial-mesenchymal transition in liver fibrosis via targeting HSP27-mediated JAK2/STAT3 and TGF-β1/Smad pathway. Phytother Res 2022;36:4167–82. https://doi.org/10.1002/ptr.7549.
[43] Zhang W, Li G, Luo R, Lei J, Song Y, Wang B, et al. Cytosolic escape of mitochondrial DNA triggers cGAS-STING-NLRP3 axis-dependent nucleus pulposus cell pyroptosis. Exp Mol Med 2022;54:129–42. https://doi.org/10.1038/s12276-022-00729-9.
[44] Lu P, Zheng H, Meng H, Liu C, Duan L, Zhang J, et al. Mitochondrial DNA induces nucleus pulposus cell pyroptosis via the TLR9-NF-κB-NLRP3 axis. J Transl Med 2023;21. https://doi.org/10.1186/s12967-023-04266-5.
[45] Chen J, Yang X, Feng Y, Li Q, Ma J, Wang L, et al. Targeting ferroptosis holds potential for intervertebral disc degeneration therapy. Cells 2022;11. https://doi.org/10.3390/cells11213508.
[46] Zhou LP, Zhang RJ, Jia CY, Kang L, Zhang ZG, Zhang HQ, et al. Ferroptosis: a potential target for the intervention of intervertebral disc degeneration. Front Endocrinol 2022;13:1042060. https://doi.org/10.3389/fendo.2022.1042060.
[47] Zou L, Huang J, Zhang Q, Mo H, Xia W, Zhu C, et al. The humanin analogue (HNG) alleviates intrauterine adhesions by inhibiting endometrial epithelial cells ferroptosis: a rat model-based study. Hum Reprod 2023;38:2422–32. https://doi.org/10.1093/humrep/dead196.
[48] Li H, Huang L, Zhao R, Wu G, Yin Y, Zhang C, et al. TSP-1 increases autophagy level in cartilage by upregulating HSP27 which delays progression of osteoarthritis. Int Immunopharmacol 2024;128:111475. https://doi.org/10.1016/j.intimp.2023.111475.
[49] Dai Y, Hu L. HSPB1 overexpression improves hypoxic-ischemic brain damage by attenuating ferroptosis in rats through promoting G6PD expression. J Neurophysiol 2022;128:1507–17. https://doi.org/10.1152/jn.00306.2022.
[50] Seo I, Kim S-W, Hyun J, Kim Y-J, Park HS, Yoon J-K, et al. Enhancing viability and angiogenic efficacy of mesenchymal stem cells via HSP90α and HSP27 regulation based on ROS stimulation for wound healing. Bioeng Transl Med 2023;8:e10560. https://doi.org/10.1002/btm2.10560.
[51] Martínez-Laorden E, Navarro-Zaragoza J, Milanés MV, Laorden ML, Almela P. Cardiac protective role of heat shock protein 27 in the stress induced by drugs of abuse. Int J Mol Sci 2020;21. https://doi.org/10.3390/ijms21103623.
[52] Boyd RA, Majumder S, Stiban J, Mavodza G, Straus AJ, Kempelingaiah SK, et al. The heat shock protein Hsp27 controls mitochondrial function by modulating ceramide generation. Cell Rep 2023;42:113081. https://doi.org/10.1016/j.celrep.2023.113081.
[53] Gallagher ER, Holzbaur ELF. SQSTM1/P62 promotes lysophagy via formation of liquid-like condensates maintained by HSP27. Autophagy 2023;19:3029–30. https://doi.org/10.1080/15548627.2023.2210943.
[54] Peng T, Wan W, Wang J, Liu Y, Fu Z, Ma X, et al. The neurovascular protective effect of S14g-humanin in a murine MCAO model and brain endothelial cells. IUBMB Life 2018;70:691–9. https://doi.org/10.1002/iub.1869.
[55] Wu Y, Zhang H, Guan L, Jia X, Wang M. S14G-humanin alleviates acute lung injury by inhibiting the activation of NF-κB. Aging (Albany NY) 2023;15:13865–75. https://doi.org/10.18632/aging.205267.
[56] Thapak P, Ying Z, Palafox-Sanchez V, Zhang G, Yang X, Gomez-Pinilla F. Humanin ameliorates TBI-related cognitive impairment by attenuating mitochondrial dysfunction and inflammation. Biochim Biophys Acta, Mol Basis Dis 2024;1870:166937. https://doi.org/10.1016/j.bbadis.2023.166937.
[57] Chai G-S, Duan D-X, Ma R-H, Shen J-Y, Li H-L, Ma Z-W, et al. Humanin attenuates Alzheimer-like cognitive deficits and pathological changes induced by amyloid β-peptide in rats. Neurosci Bull 2014;30:923–35. https://doi.org/10.1007/s12264-014-1479-3.
[58] Nashine S, Cohen P, Wan J, Kenney MC. Effect of Humanin G (HNG) on inflammation in age-related macular degeneration (AMD). Aging (Albany NY) 2022;14:4247–69. https://doi.org/10.18632/aging.204074.
[59] Hashimoto Y, Takeshita Y, Naito M, Uchino H, Matsuoka M. Apollon/Bruce is upregulated by Humanin. Mol Cell Biochem 2014;397:147–55. https://doi.org/10.1007/s11010-014-2182-4.
[60] Gao GS, Li Y, Zhai H, Bi JW, Zhang FS, Zhang XY, et al. Humanin analogue, S14G-humanin, has neuroprotective effects against oxygen glucose deprivation/reoxygenation by reactivating Jak2/Stat3 signaling through the PI3K/AKT pathway. Exp Ther Med 2017;14:3926–34. https://doi.org/10.3892/etm.2017.4934.
[61] Zhang G-Z, Liu M-Q, Chen H-W, Wu Z-L, Gao Y-C, Ma Z-J, et al. NF-κB signalling pathways in nucleus pulposus cell function and intervertebral disc degeneration. Cell Prolif 2021;54:e13057. https://doi.org/10.1111/cpr.13057.
[62] Navone SE, Marfia G, Giannoni A, Beretta M, Guarnaccia L, Gualtierotti R, et al. Inflammatory mediators and signalling pathways controlling intervertebral disc degeneration. Histol Histopathol 2017;32:523–42. https://doi.org/10.14670/HH-11-846.
[63] Li H, Yang P, Wang J, Zhang J, Ma Q, Jiang Y, et al. HLF regulates ferroptosis, development and chemoresistance of triple-negative breast cancer by activating tumor cell-macrophage crosstalk. J Hematol Oncol 2022;15:2. https://doi.org/10.1186/s13045-021-01223-x.
[64] Cao F, Li M, Wang W, Yi Y, Chen Y, Liu H. A coumarin-furoxan hybrid as novel nitric oxide donor induced cell apoptosis and ferroptosis in NSCLC by promoting S-nitrosylation of STAT3 and negative regulation of JAK2-STAT3 pathway. Biochem Pharmacol 2024;222:116068. https://doi.org/10.1016/j.bcp.2024.116068.
[65] Wang Y, Liu J, Kong Q, Cheng H, Tu F, Yu P, et al. Cardiomyocyte-specific deficiency of HSPB1 worsens cardiac dysfunction by activating NFκB-mediated leucocyte recruitment after myocardial infarction. Cardiovasc Res 2019;115:154–67. https://doi.org/10.1093/cvr/cvy163.
[66] Sims JT, Ganguly SS, Bennett H, Friend JW, Tepe J, Plattner R. Imatinib reverses doxorubicin resistance by affecting activation of STAT3-dependent NF-κB and HSP27/p38/AKT pathways and by inhibiting ABCB1. PLoS One 2013;8:e55509. https://doi.org/10.1371/journal.pone.0055509.
[67] Song Y, Lu S, Geng W, Feng X, Luo R, Li G, et al. Mitochondrial quality control in intervertebral disc degeneration. Exp Mol Med 2021;53:1124–33. https://doi.org/10.1038/s12276-021-00650-7.

[68] Lin MT, Beal MF. Mitochondrial dysfunction and oxidative stress in neurodegenerative diseases. Nature 2006;443:787–95.
[69] Su B, Li R, Song F, Liu M, Sun X. S14G-Humanin ameliorates ovalbumin-induced airway inflammation in asthma mediated by inhibition of toll-like receptor 4 (TLR4) expression and the nuclear factor κ-B (NF-κB)/early growth response protein-1 (Egr-1) pathway. Aging (Albany NY) 2023;15:6822–33. https://doi.org/10.18632/aging.204874.
[70] Song Y, Lu S, Geng W, Feng X, Luo R, Li G, et al. Mitochondrial quality control in intervertebral disc degeneration. Exp Mol Med 2021;53:1124–33. https://doi.org/10.1038/s12276-021-00650-7.
[71] Song C, Xu Y, Peng Q, Chen R, Zhou D, Cheng K, et al. Mitochondrial dysfunction: a new molecular mechanism of intervertebral disc degeneration. Inflamm Res 2023;72:2249–60. https://doi.org/10.1007/s00011-023-01813-0.
[72] Kumagai H, Miller B, Kim SJ, Leelaprachakul N, Kikuchi N, Yen K, et al. Novel insights into mitochondrial DNA: mitochondrial microproteins and mtDNA variants modulate athletic performance and age-related diseases. Genes 2023;14. https://doi.org/10.3390/genes14020286.
[73] Lei H, Rao M. The role of humanin in the regulation of reproduction. Biochim Biophys Acta Gen Subj 2022;1866:130023. https://doi.org/10.1016/j.bbagen.2021.130023.
[74] Xiang H, Zhao W, Jiang K, He J, Chen L, Cui W, et al. Progress in regulating inflammatory biomaterials for intervertebral disc regeneration. Bioact Mater 2024;33:506–31. https://doi.org/10.1016/j.bioactmat.2023.11.021.
[75] Yu Y, Pang Z, Lu W, Yin Q, Gao H, Jiang X. Self-assembled polymersomes conjugated with lactoferrin as novel drug carrier for brain delivery. Pharm Res (N Y) 2012;29:83–96. https://doi.org/10.1007/s11095-011-0513-7.
[76] Solanki A, Smalling R, Parola AH, Nathan I, Kasher R, Pathak Y, et al. Humanin nanoparticles for reducing pathological factors characteristic of age-related macular degeneration. Curr Drug Deliv 2019;16:226–32. https://doi.org/10.2174/1567201815666181031163111.
[77] Keorochana G, Johnson JS, Taghavi CE, Liao J-C, Lee K-B, Yoo JH, et al. The effect of needle size inducing degeneration in the rat caudal disc: evaluation using radiograph, magnetic resonance imaging, histology, and immunohistochemistry. Spine J : official journal of the North American Spine Society 2010;10:1014–23. https://doi.org/10.1016/j.spinee.2010.08.013.